Local genomic estimates provide a powerful framework for haplotype discovery

Will Shaffer[1], Victor Papin [1], Seema Yadav [1], Kai P. Voss-Fels [1,2], Lee T. Hickey [1], Ben J. Hayes [1], Eric G. Dinglasan[1*]

[1]Queensland Alliance for Agriculture and Food Innovation, The University of Queensland, Brisbane, Queensland, 4072, Australia

[2]Institute of Plant Breeding, Hochschule Geisenheim University, 65366 Geisenheim, Germany

[*]Correspondence: Eric Dinglasan (e.dinglasan@uq.edu.au)

Running title: Local genomic estimates for haplotype discovery

Abstract

Quantitative trait loci (QTL) discovery studies on diversity panels or breeding populations typically use genome-wide association studies (GWAS) to estimate marker effects. For plant and animal breeding applications, researchers increasingly recognize the potential benefits of identifying superior haplotypes (markers in linkage disequilibrium; LD) rather than relying on single markers, as traditional approaches inefficiently account for cumulative signals from incomplete LD with QTL or split effects when multiple markers are in high LD with QTL. Using the genomic prediction framework, the local genomic estimated breeding values (localGEBV) method was developed in animal breeding and has been adopted in crop haplotype mapping studies; however, no study has thoroughly quantified the utility of this method or systematically compared outcomes to traditional GWAS approaches. Here, we characterized a strategy to group markers in chromosomal segments based on LD (haplotype blocks or haploblocks), computed localGEBV as a linear contrast of marker effects within each haploblock, and utilised the variance of localGEBV to enhance QTL discovery compared to traditional GWAS. Marker effects for localGEBV were estimated with ridge-regression best linear unbiased prediction (rrBLUP) and BayesR, with results compared to two common GWAS approaches. Using the barley row-type trait, we demonstrated that localGEBV improved QTL discovery and phenotypic prediction compared to single markers. Furthermore, localGEBV results were robust to the choice of prior marker assumptions and blocking parameters, enabling flexibility in fine or broad-scale QTL mapping. Overall, our findings establish localGEBV as a haplotype-based strategy capable of leveraging localized genomic effects to improve QTL discovery and, potentially, genomic selection.

Key words: local GEBV, linkage disequilibrium, GWAS, genomic selection, haplotype, haploblock

Introduction

Understanding the genetic basis of trait variation is fundamental to advancing crop and livestock improvement programs. Identifying quantitative trait loci (QTL) or genomic regions harbouring mutations that contribute to trait variation provides crucial insights into genetic architecture and enables targeted breeding strategies. Traditional genome-wide association studies (GWAS) detect QTL by testing associations between individual genetic markers and phenotypes using linear regression, while modern approaches utilize linear mixed models, Bayesian hierarchical models, or multi-stage methods. A significant association indicates the marker is in linkage disequilibrium (LD) with a causal mutation.

The single-marker approach proves effective in populations with limited LD, such as human populations with large effective population sizes. However, this approach lacks precision in populations characterized by more extensive LD due to small effective population sizes – a common feature of crop and livestock populations. In these populations, markers that are in LD often split the QTL effect when estimated simultaneously, and individual markers may capture only fragments of the total QTL effect through imperfect LD relationships (Meuwissen and Goddard, 2000; Marchini et al., 2004; Goddard, 2009; Zhang et al., 2010). This dilution of signal across multiple correlated markers reduces the power to detect causal variants.

To address these limitations, chromosome segments in LD can be leveraged through haplotype-based approaches that capture the collective signal across multiple linked markers (Meuwissen and Goddard, 2000; The Bovine HapMap Consortium et al., 2009; Comadran et al., 2011; Joukhadar et al., 2017). These methods group markers into haplotype blocks, typically defined as LD-based chromosomal segments (LD blocks or haploblocks), and analyse the combined effects within each block. One promising haplotype-based method utilizes the variance of local genomic estimated breeding values (localGEBV), which represents the variance of haplotype effects within a block. This approach has demonstrated the ability to detect QTL where causal mutations are known in livestock populations (Fan et al., 2011; Kemper et al., 2015; Van Den Berg et al., 2019; Xiang et al., 2021). Unlike traditional GWAS that tests markers individually, the localGEBV approach, derived from genomic prediction methods, begins with fitting all single nucleotide polymorphism (SNP) simultaneously (Meuwissen et al., 2001), counteracting shrinkage effects and the dilution of marker effects when multiple markers tag the same QTL. Theoretical advantages of the localGEBV approach include reduced susceptibility to false positives from population

stratification, less severe over-estimation of effects, and improved QTL detection power, all stemming from the simultaneous fitting of all SNP rather than individual testing (Yang et al., 2014).

The localGEBV method has also shown promise in crop applications. Voss-Fels et al. (2019) first applied this approach in wheat to identify beneficial haplotypes for yield, though their focus was on breeding program improvements rather than QTL discovery methodology. Others have applied the same method to identify haplotypes important for disease resistance in barley and wheat (Tong et al., 2024; Roy et al., 2025; Vo Van-Zivkovic et al., 2025), stay-green and root traits in barley (Brunner et al., 2024; Alahmad et al., 2025; Aldiss et al., 2025), and chickpea seed weight, flowering time, and plant height (Varshney et al., 2021; Akinlade et al., 2025).

Despite these promising developments, critical knowledge gaps limit our understanding and application of haplotype-based QTL detection. No direct comparison between localGEBV and standard GWAS approaches has been conducted to empirically evaluate their relative performance. Previous applications in QTL discovery in livestock have relied on sliding window approaches, whereas in crop species, haplotype discovery focused on biologically meaningful LD-based blocks. However, the effect of fundamental methodological aspects, including optimal marker effect priors and blocking parameters, remain poorly characterized for QTL discovery.

Here, we address these gaps through comprehensive evaluation of the localGEBV approach using a barley global diversity panel genotyped with 40K SNP, focusing on spike row morphology, a trait with complex genetic architecture distinguishing 2-row from 6-row varieties. We construct LD-based haploblocks, investigate localGEBV estimation using ridge regression best linear unbiased prediction (rrBLUP) and BayesR to account for different marker effect priors (Meuwissen et al., 2001; Erbe et al., 2012), and directly compare QTL detection capabilities against established multi-locus GWAS methods (FarmCPU and BLINK). Our findings demonstrate that haplotype-based localGEBV offers superior precision and power for QTL discovery in populations with extensive LD by detecting multiple known QTL compared to modern GWAS methods, providing a robust framework applicable across plant and animal breeding programs.

Results

Barley accessions display distinct genetic differentiation for row-type phenotypes

Principal component analysis revealed substantial genetic differentiation among the barley accessions, with PC1 and PC2 explaining 30.4% and 14.4% of variation, respectively. *K-means* clustering identified three main genetic clusters (Figure 1A): Cluster 1 (313) comprised predominantly 2-row accessions, while Clusters 2 (297) and 3 (180) were primarily composed of 6-row accessions (Figure 1B and 1D).

LD analysis demonstrated high initial LD ($r^2 = 0.74$) within distances <0.1 Mbp, followed by rapid decay to $r^2 = 0.19$ at 1 Mbp, with subsequent gradual decay thereafter (Figure 1C).

LD-based haploblock construction reveals diverse genomic segmentation patterns

The construction of chromosome segments using varying LD parameters generated distinct haploblock configurations. Relaxed parameters (lower r^2 threshold and higher marker tolerance, tol, which allowed some markers in the block to not meet the LD threshold) generated fewer haploblocks total with more markers per haploblock, while stringent parameters (higher r^2 threshold, lower marker tolerance) produced more numerous haploblocks that were predominantly single-marker blocks (Supplementary Figure 1). For instance, at $r^2 = 0.1$ with zero marker tolerance, 3,738 haploblocks (447,691 possible haplotypes) were constructed, with 60.27% comprising single SNP markers. Increasing the r^2 threshold to 0.5 resulted in 6,781 haploblocks (103,857 possible haplotypes), where 73.72% consisted of single SNP markers.

Increasing marker tolerance substantially reduced haploblock count while expanding block size and possible haplotype numbers. At $r^2 = 0.1$ with marker $tol = 3$, only 1,096 haploblocks were constructed (2,890,043 possible haplotypes). The largest observed haploblock (364 SNP markers spanning 299 Mbp on chromosome 5H) contained 374,192 possible haplotypes.

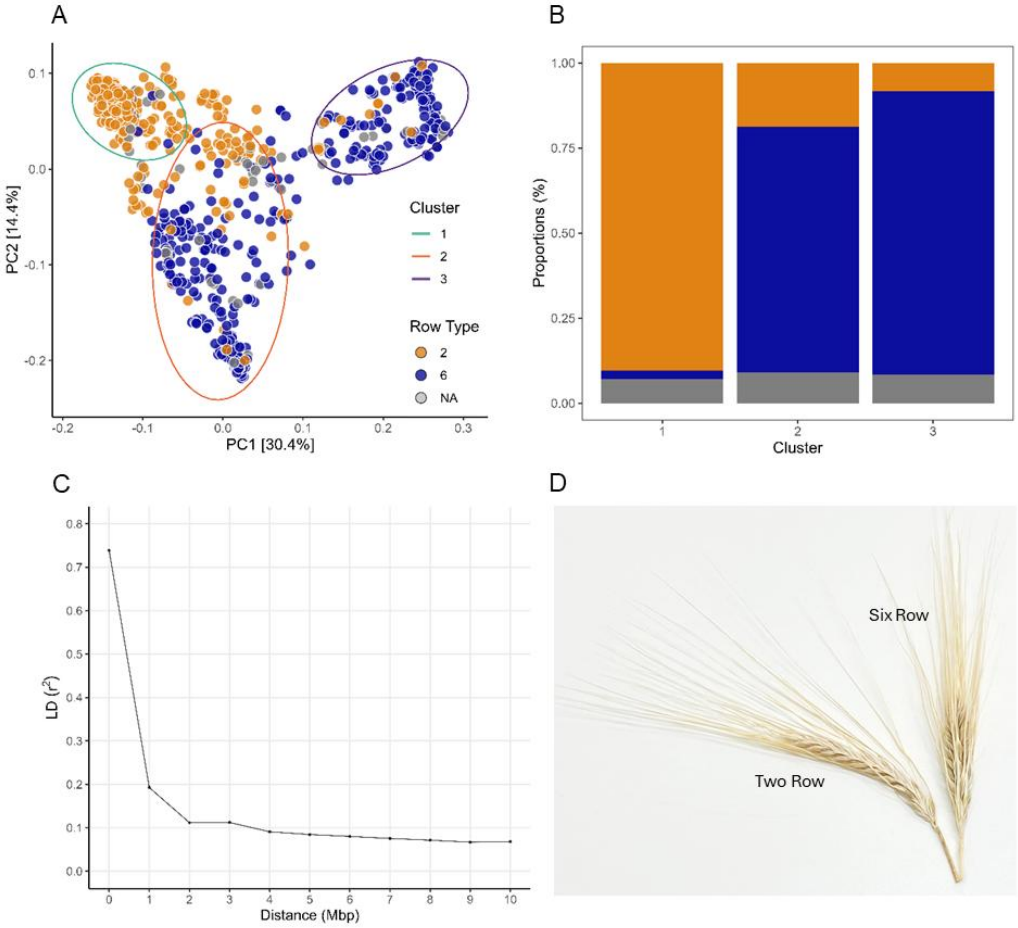

Figure 1. **Population structure and genetic relationships of barley germplasm.** (**A**) Principal component analysis of *N* = 790 barley accessions using 9,050 XT SNP chip markers, revealing three distinct genetic clusters. Shown are PCs 1 and 2 from Roger's genetic distance matrix, accounting for 44.8% cumulative explained variation. The optimum number of clusters were *clusters* = 3: Cluster 1 (313), Cluster 2 (297), and Cluster 3 (180). *Colours* represent the row spike phenotype i.e. 2-row is *orange*, 6-row is *blue*. (**B**) Proportions of barley accessions across the three clusters: Cluster 1 (2-row = 283, 6-row = 8, NA = 22), Cluster 2 (2-row = 56, 6-row = 214, NA = 27), Cluster 3 (2-row = 15, 6-row = 150, NA = 15), where NA represents accessions with ambiguous information and 'irregular' type. (**C**) Genome-wide LD decay as a function of physical distance (Mbp). LD decay is shown at an average distance (Mbp) between adjacent SNP based on the XT SNP chip physical position using cv Morex assembly v2 and visualised up to 10 Mbp. (**D**) An example of the two-row and six-row phenotypes.

Validation of localGEBV approach for mapping *VRS1* gene in chromosome 2H

To determine whether haploblock variance was influenced by segment size, we applied a generalized additive linear regression model, which revealed no meaningful linear relationship between haploblock variance and block size (number of markers; $R^2 = 0.07$, $P <$ 2e-16; Figure 2, Supplementary Figure 3). Instead, a significant and meaningful relationship was observed between haploblock variance and haplotype effects ($R^2 = 0.48$, $P <$ 2e-16).

We validated the localGEBV approach by examining the well-characterized *VRS1* gene on chromosome 2H, which determines row-type phenotype (Komatsuda et al., 2007). Marker effect estimation using rrBLUP showed relatively small effects distributed across the chromosome, with modest increase in the *VRS1* region (Supplementary Figure 2). In contrast, BayesR attributed larger effects to SNP collocated with *VRS1* compared to surrounding markers. Analysis of localGEBV variance across different LD parameters consistently identified haploblocks peaking at the *VRS1* region (Figure 3A). Both rrBLUP and BayesR detected maximum variance at $r^2 = 0.1$ and marker tolerance, $tol = 3$, co-locating with *VRS1* and with localGEBV variance of 0.0081 and 0.0133, respectively (Figure 3A; Table 1).

Closer examination of the highest variance haploblock in chromosome 2H identified progressive refinement from 49 SNP spanning 10.23 Mbp at $r^2 = 0.1$ to 4 SNP spanning 0.88 Mbp at $r^2 = 0.5$ (Figure 3B), denoting the trade-off between flexibility of block discovery power and fine-mapping resolution with choice in blocking parameters. BayesR consistently produced higher variance estimates at the *VRS1* region compared to rrBLUP, likely due to its heterogeneous variance assumptions allowing larger effects for SNP in high LD with QTL. Additionally, rrBLUP identified dispersed regions of additional high variance haploblocks in chromosome 2H, particularly within 231.42 to 431.25 Mbp when using relaxed LD parameters. These regions diminished in BayesR at higher LD thresholds, consistent with its assumption that most SNP have no effect on the trait (Supplementary Figure 2).

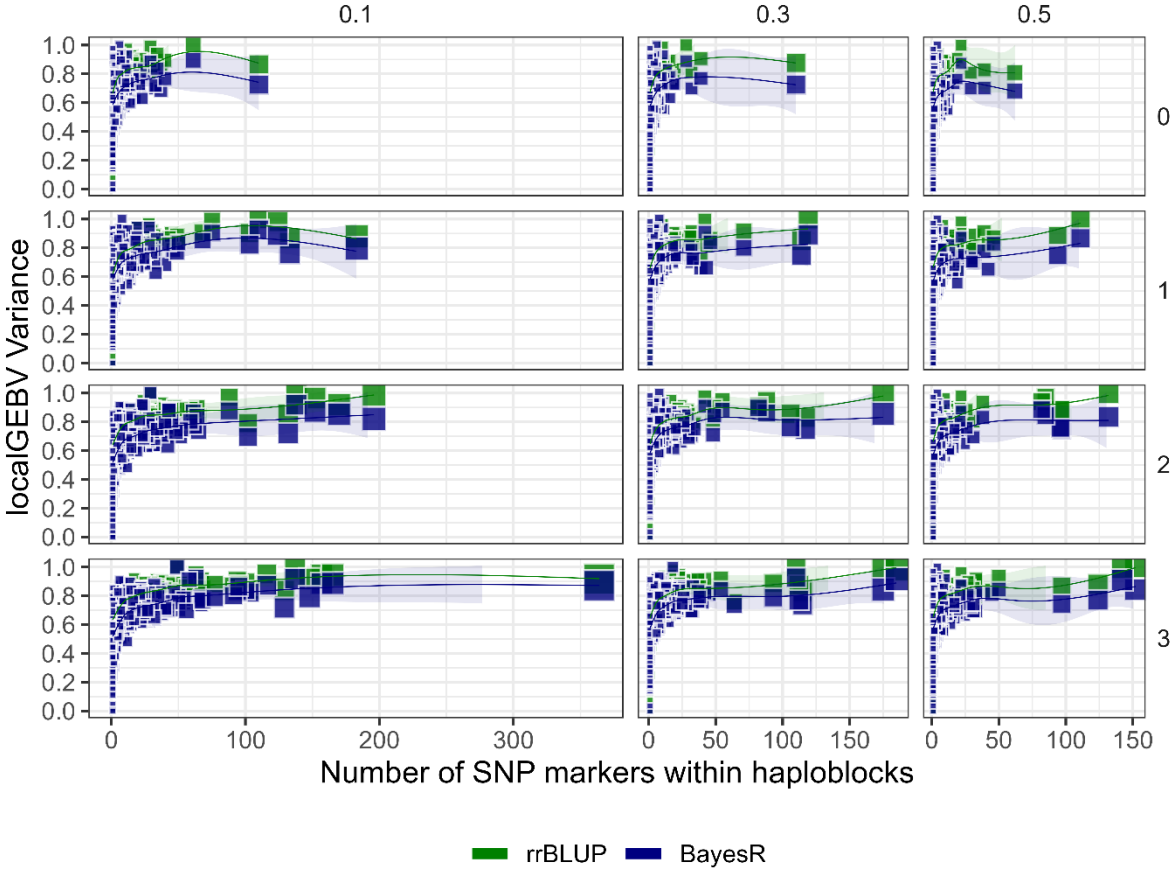

Figure 2. Relationship between haploblock variance and haploblock size. Haploblock variance derived from localGEBV estimates using rrBLUP (*green*) and BayesR (*blue*), plotted on the *y-axis*. Block size is defined by the number of SNP markers within haploblocks, plotted on the *x-axis*. In the figure, different LD parameters are shown as facets: *column facets* represent LD thresholds of $r^2 \in \{0.1, 0.3, 0.5\}$; and *row facet* as marker tolerance, $tol \in \{0, 1, 2, 3\}$. The localGEBV variance was scaled using a min-max scaling of the $\log_{10}$ transformed variance. Blocks were connected using a generalized additive model for non-linear relationships to represent trends between haploblock size and localGEBV variance.

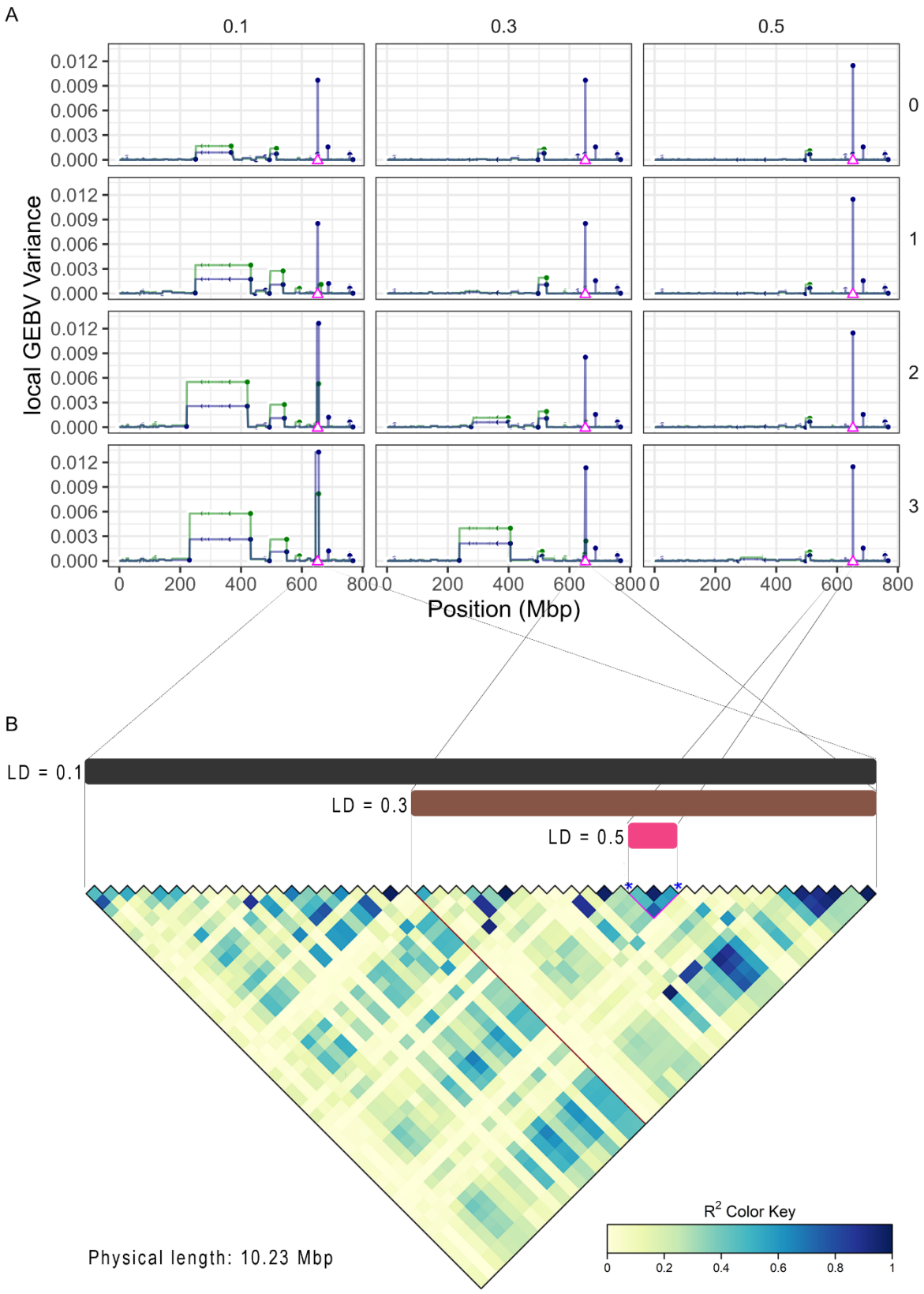

Figure 3. LocalGEBV variance of haploblocks in chromosome 2H. The *VRS1* gene (marked as Δ) is co-located at 652.03 Mbp based on the XT SNP chip physical position using cv Morex assembly v2. (**A**) The localGEBV variance profiles across chromosome 2H

estimated using rrBLUP (*green*) or BayesR (*blue*). Haploblocks are constructed according to different LD parameters: where *column facet* represents LD threshold at $r^2 \in \{0.1, 0.3, 0.5\}$; and *row facet* as $tol \in \{0, 1, 2, 3\}$. (**B**) Varying sizes of the haploblocks based on LD threshold show fine-scale mapping in the *VRS1* region. Haploblocks constructed at $r^2 \in \{0.1, 0.3, 0.5\}$ with $tol \in \{0, 1, 2, 3\}$. Shown together is the corresponding LD heatmap.

Ability of localGEBV to detect QTL

We first assessed QTL detection using the mean haploblock variance and the blocking parameters that maximised the haploblock variance at the *VRS1* locus, which corresponded to blocking parameters of $r^2 = 0.1$ and $tol = 3$. With these parameters, we identified $rrBLUP = 158$ and $BayesR = 136$ high-variance haploblocks that surpassed the mean haploblock variance from the total of $J = 1096$ haploblocks (Figure 6), of which 96 were in common.

We then employed a chi-squared distribution to generate Bonferroni and False Discovery Rate (FDR) probability values (Table 1). At an FDR critical value of 0.05, $rrBLUP = 16$ and $BayesR = 15$ haploblocks were identified as significant. Comparative GWAS analysis using FarmCPU and BLINK identified 6 significant markers: 5 on chromosome 2H (2 detected by both methods) and 1 on 4H (FarmCPU only). Compared to the GWAS results, localGEBV identified 21 unique high variance haploblocks distributed across all chromosomes, with 10 detected by both rrBLUP and BayesR, and 6 and 5 uniquely identified by each method, respectively (Table 1, Figure 4).

Haploblock 2H:b000235 exhibited the highest localGEBV variance ($rrBLUP = 0.0082$; $BayesR = 0.0133$). This haploblock (spanning 645.10 to 655.33 Mbp) contained all 4 significant markers detected by GWAS, including the most significant marker 2H:AVRIG03047 ($-\log_{10} P_{adj}$; FarmCPU = 17.6, BLINK = 10.5) at 652.42 Mbp, co-locating with the *VRS1* gene (Komatsuda et al., 2007; Table 1, Figure 4).

Notably, the localGEBV approach identified additional high variance haploblocks significant after Bonferroni or FDR correction that collocated with known genes and candidate genes related to row phenotype. Both rrBLUP and BayesR identified haploblocks 1H:b000049, 3H:b000382, 4H:b000552, and 7H:b001032 co-locating with *VRS3* (associated with grain uniformity; Van Esse et al., 2017; Bull et al., 2017), *HORVU3Hr1G036930* (linked to lateral

204 spikelet fertility; Youssef et al., 2020), and lateral spike fertility (*VRS5* and
205 *HORVU7Hr1G090180*; Ramsay et al., 2011; Youssef et al., 2020) respectively. BayesR
206 uniquely identified haploblock 1H:b000091, co-locating with the QTL associated with "third
207 outer glume" structure (TRD). None of these blocks contained significant markers in the
208 FarmCPU and BLINK analyses.

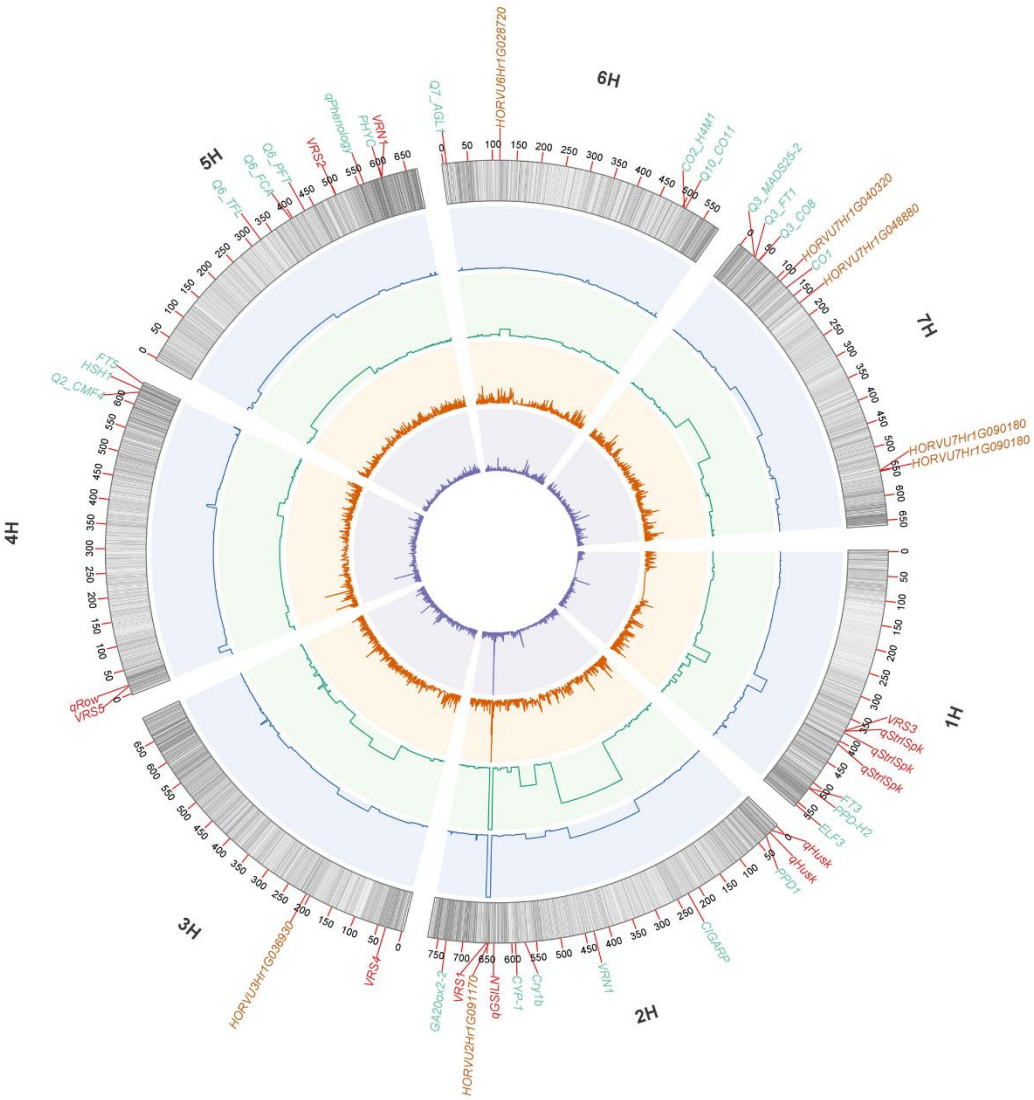

Figure 4. Detection of haploblocks containing QTL. Physical position in barley chromosome of SNP markers associated with row-type spike architecture detected from localGEBV and GWAS**.** ***Tracks 1 to 5 (outer to innermost):*** **Track 1** Barley chromosome showing physical position (Mbp) based on cv Morex assembly v2 from the 40K XT SNP chip. SNP markers are coloured in *grey*. Colocation of known genes and QTL from the literatures is shown: row-type known genes (*VRS3* in 1H, *VRS1* in 2H, *VRS4* in 3H, *VRS5* in 4H, *VRS2* in 5H; *dark red*), phenology genes (*FT3*, *PPD1*, *CIGARP*, *Cry1b*, *CYP-1*, *GA20ox2*-2, Q2_*CMF4*, *HSH1*, *FT5*, Q6_*TFL*, Q6_*FCA*, *Q6_PFT*, *PHYC*, *Q7_AGL1*, *CO2_H4M1*, *Q10_CO11*, *Q3_MADS25-2*, *Q3_FT1*, *Q3_CO8*, *CO1*; *green*), yield-component candidate genes (*brown*); and QTL for spike sterility (qStrlSpk), grain spiculation of inner lateral nerve (qGSILN), spike row number (qRow), are also shown in *dark red*. **Track 2** LocalGEBV estimated using Bayes R, track colour in *blue*. **Track 3** LocalGEBV estimated using rrBLUP, track colour in *green*. **Track 4** GWAS using BLINK, track colour in

orange. **Track 5** GWAS using FarmCPU, track colour in *purple*. In both **Track 2** and **Track 3**, localGEBV haploblocks were according to LD blocking parameters: LD threshold $r^2 = 0.1$ and marker $tol = 3$; and shown is the variance localGEBV according to the position of flanking markers within haploblocks. In both **Track 4** and **Track 5**, markers were considered significant according to thresholds after FDR corrections ($-\log_{10} P_{adj} > -\log_{10} 0.008$ for FarmCPU and $-\log_{10} P_{adj} > -\log_{10} 0.004$ for BLINK).

Haploblocks demonstrate superior predictability compared to single markers

Using a classical linear model and generalized linear model framework, we aimed to demonstrate that the discrete, categorical haplotype configurations (i.e., discretised localGEBV values) had greater ability to predict row-type phenotype compared to discrete, categorical single marker genotypes. We first conducted principal component analysis on the marker effects from each method of estimating marker effects and conducting GWAS (FarmCPU, BLINK, rrBLUP, and Bayes R). Principal component analysis of marker effect estimates from all methods showed PC1 and PC2 explaining 73.93% of cumulative explained variance, with marker 2H:AVRIG03047 contributing most substantially (17.49%), followed by 4H:AVRIG07945 (5.64%; Figure 5A). Marker 2H:AVRIG03047 was part of the haploblock collocating with the *VRS1* gene and identified as significant by all GWAS and haploblocking strategies (Table 1), whereas marker 4H: AVRIG07945 was only identified in haploblock b000636 using BayesR marker effects.

We further evaluated the regression of row-spike status on SNP genotypes or localGEBV haplotype configurations fit as categorical effects for row-spike phenotype prediction accuracy utilising both a linear probability model (LPM) and logistic regression in a generalized linear model (GLM) framework. Configurations were fit as categorical predictors to capture non-additive effects and to avoid utilizing the localGEBV and marker effect values trained on the whole population. This ensured that the predicted effects were specific to the sampled training set. The SNP-only model (mAVRIG03047) used the single most significant marker identified in the FarmCPU/BLINK, while the other two models (rrBLUP.b000235 and BayesR.b000235), incorporate information from haplotypes within the 2H:b000235 (r^2 = 0.1, tol = 3) simultaneously. The average of the five-fold cross-validation correlations between the predicted phenotype and actual phenotype in the test set were consistently higher for both significant markers and the highest variance haploblock compared to randomly selected markers or haploblocks (Figure 5B). Notably, both rrBLUP and BayesR achieved higher correlation values when using haploblock haplotype configurations as predictors (LPM = 0.88, GLM = 0.81; Root Mean Squared Error; RMSE LPM = 0.07, GLM = 1.78) compared to single marker genotypes (LPM = 0.75, GLM = 0.71; RMSE: LPM = 0.07, GLM = 3.31). The RMSE for the LPM utilising single markers was lower. This is likely a downwards biased estimate because of the violation of ordinary least squares assumptions and should not be utilised to justify a better model fit than the logistic regression model.

Haplotype analysis reveals distinctive features of localGEBV

We explored the relationship between haploblock variance and the effect of individual haplotypes (Figure 6). In general, as the magnitude of a localGEBV increased, the variance of the corresponding block was greater (Figure 6, Supplementary Figure 3).

Detailed haplotype profiling of haploblock 2H:b000235 (*VRS1* region) at higher LD resolution ($r^2 = 0.5, tol = 3$) revealed 4 SNP markers spanning 0.88 Mbp (651.54 to 652.42 Mbp) with varying allele frequencies (Figure 7B). From these markers, 30 haplotypes were identified, with 13 occurring at frequencies ≥5 accessions. Two predominant haplotypes emerged as complete allelic reversals: hap1 (TTTT) associated primarily with 2-row phenotype (252) and hap2 (AAAA) with 6-row phenotype (239).

Haplotype network analysis demonstrated that the direction of haplotype effects aligned with phenotypic expression: negative effects for hap1 is associated with 2-row and positive effects for hap2 is linked with 6-row (Figures 6, 7C); this aligns with the regression analysis in accurately predicting 2-row or 6-row phenotypes utilising the same haplotype effects (Figure 5B). Hierarchical clustering based on similarity matrix scores differentiated distinct clusters corresponding to haplotype-phenotype associations, wherein Australian Grains Genebank (AGG) accessions carrying hap1 had 2-row spikes while AGG accessions with hap2 had 6-row spikes (Figure 7D).

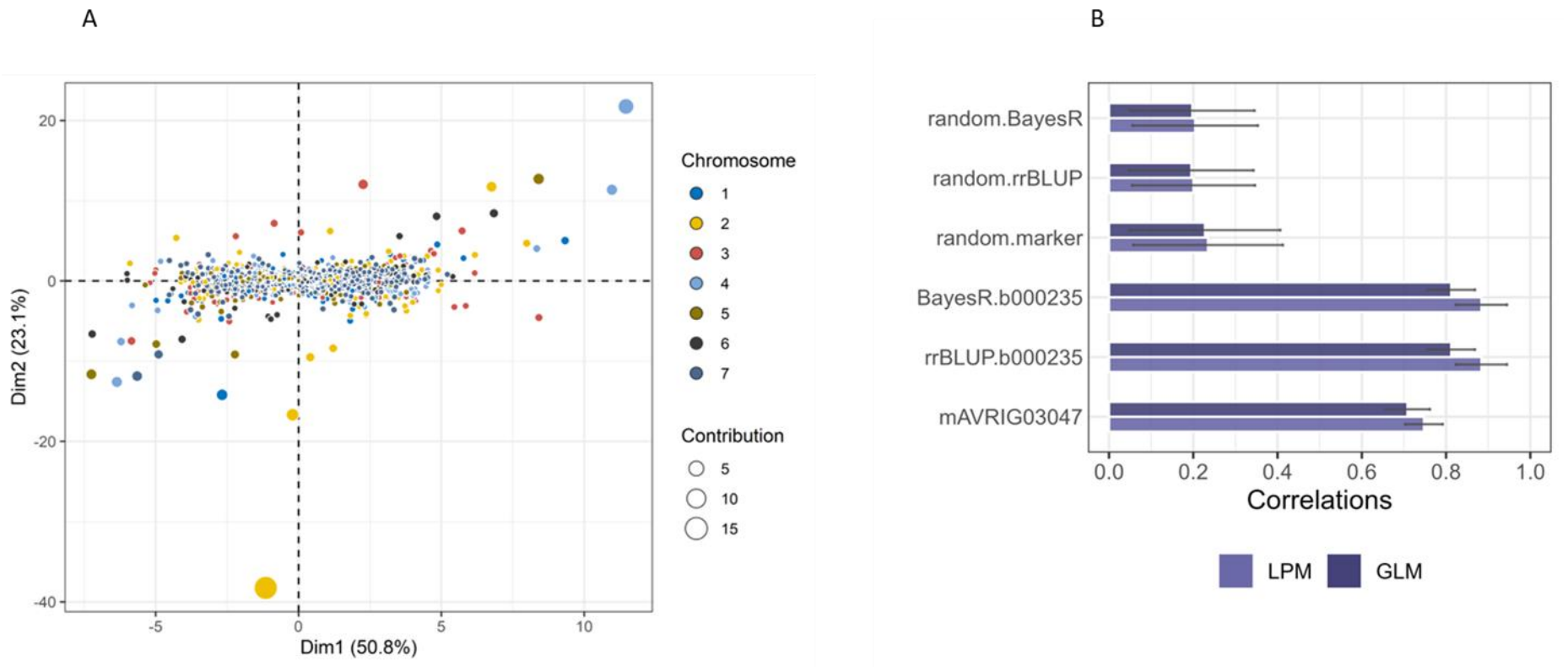

Figure 5. Accuracy of predictors in identifying informative associations with row-spike phenotype. (**A**) Principal component analysis showing the effects contribution of M = 9,050 XT SNP marker estimates from FarmCPU, BLINK, rrBLUP, and BayesR. *Colours* represent the 7 barley chromosomes; *size* of each dots represents the SNP effect contribution to the principal components relating to row-spike phenotype. (**B**) Regression analysis of marker genotypesor haploblock haplotype configurations as predictors. Shown is the accuracy calculated as correlations of the predicted value in the testing set; predicted values calculated using ordinary least squares linear probability model (LPM, *light purple*) and logistic regression in the generalised linear model (GLM, *dark purple*). The most significant marker (2H:AVRIG03047) identified by both

286 FarmCPU and BLINK and the haploblock with the highest variance from rrBLUP and BayesR localGEBV estimates (2H:b000235) were
287 analysed in each model and compared with non-significant random marker/haploblock haplotype configurations. Analyses for random
288 marker/haploblock haplotype configurations were repeated 100 times, and the average correlation and standard deviations of the 100 repetitions
289 represented as error bars were shown.

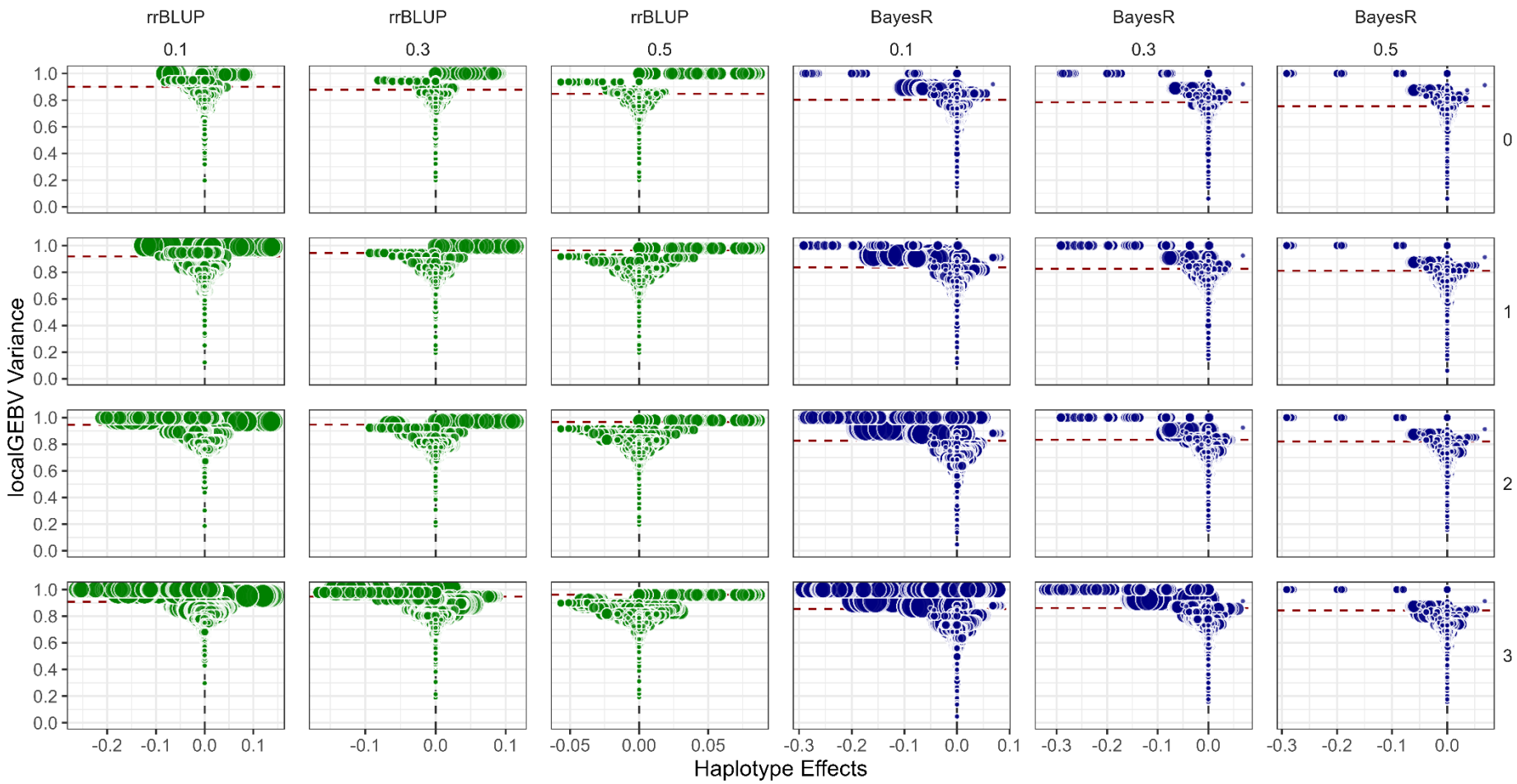

Figure 6. Relationship between haploblock variance and haplotype effects. Haploblock variance was determined from the localGEBV estimates using rrBLUP (*green*) and BayesR (*blue*); plotted as min-max scaled of the log_{10} transformed variance for visual clarity. In the figure, different LD parameters are shown as facets: *column facet* represented by LD threshold at $r^2 \in \{0.1, 0.3, 0.5\}$; and *row facet* as marker tolerance

$tol \in \{0, 1, 2, 3\}$. *Dashed horizontal lines* represent the average haploblock variance at each LD parameter, where haploblocks above the threshold are considered containing the QTL. *Size* of each circle corresponds to the number of markers within the haploblock.

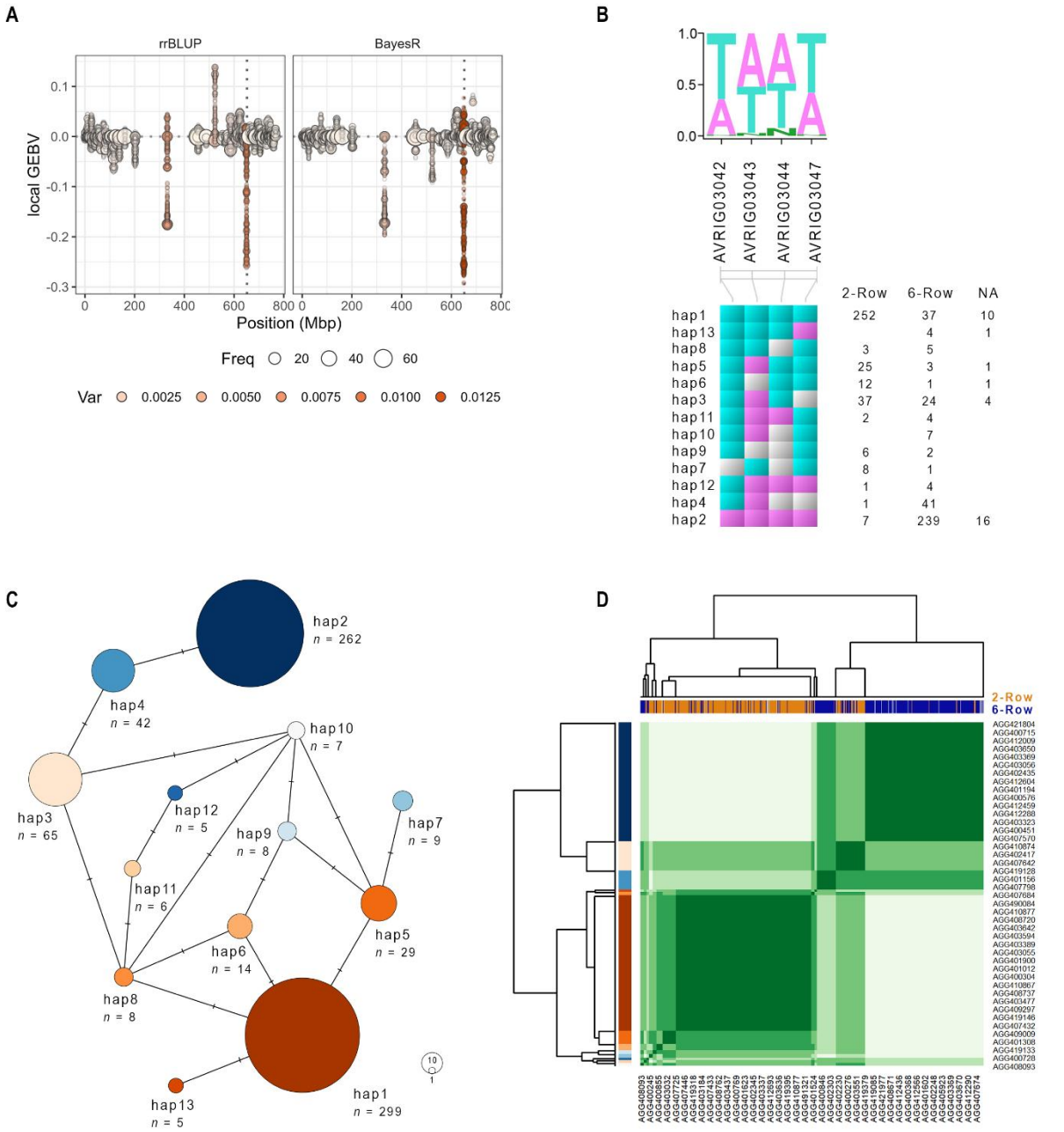

Figure 7. Haplotype analysis. (**A**) Identification of haplotypes from the localGEBV estimates using rrBLUP and BayesR. In the figure, *x-axis* shows the marker physical position (Mbp) of chromosome 2H based on cv Morex assembly v2 from the 40K XT SNP chip; while the *y-axis* corresponds to localGEBV or haplotype effects. The *dotted vertical line* illustrates the position of *VRS1* gene at 652.03 Mbp. Haplotypes associated with row-type phenotypes are determined by the direction of localGEBV estimates, whereby negative localGEBV effects favours 2-row phenotypes while positive localGEBV effects favours 6-row phenotypes. Each *dot* corresponds to a specific haplotype, wherein the *size* of the dots represents the haplotype abundance or the frequency of barley accessions carrying the

haplotype; while *orange colour gradient* represents higher haploblock variance. (**B**) Haplotype profile collocating *VRS1* gene. Shown is the 0.88 Mbp finer region within 2H:b00023 defined by four markers (i.e. AVRIG03042, AVRIG03043, AVRIG03044, AVRIG03047; spanning 651.54 to 652.42 Mbp); wherein, arbitrarily, *A* corresponds to the reference allele, *T* corresponds to the alternate allele, and a missing allele is represented by *N*. Marker AVRIG03047 was also the most significant marker identified by FarmCPU ($-\log_{10} P_{adj} = 17.59$) and BLINK ($-\log_{10} P_{adj} = 10.49$). The *top panel* shows the estimated density of alleles at each four marker positions, while the *bottom panel* shows the 13 haplotypes identified and their frequency of occurrence across barley accessions relative to each row-type phenotype. Only haplotypes with a frequency *of at least* 5 accessions are shown. **(C**) Haplotype network analysis. Shown is a statistical parsimony network (TCS method; Templeton et al., 1992) of the 13 haplotypes. The *size* of the circle is proportional to the number of barley accessions carrying the respective haplotypes, while the *hash marks* indicate the number of mutational steps. *Colour gradient* illustrates the localGEBV or haplotype effects, with *dark orange* and *dark blue* indicating the lowest (i.e. negative) and highest (i.e., positive) haplotype effects, respectively. (**D**) Heatmap of similarity matrix score of the haplotypes among 759 barley accessions. In the figure, barley accessions are separated into two major clusters according to complete linkage hierarchical clustering, wherein the *top colour bar* represents the row-spike phenotypes of the barley accession (i.e., 2-row in *orange* and 6-row in *blue*) while the *left colour bar* represents the 13 haplotypes described in panels B and C.

Discussion

In this study, we demonstrated that localGEBV offers substantial improvements in QTL discovery compared to standard GWAS methods. By integrating LD information with genomic prediction models, the framework effectively partitions the genome into disjointed chromosome segments with estimated haplotype effects (localGEBV) and haploblock variances. This allowed us to leverage local information in the genome enabling more comprehensive detection of genetic loci controlling complex traits. Furthermore, we assessed the impact different marker tolerance and LD threshold blocking parameters had on discovery to provide a general guideline on how to conduct blocking.

Biological complexity of barley row-type phenotype as a model for QTL discovery

The barley row-type phenotype represents an ideal model for testing QTL discovery methods due to its simple phenotype and semi-complex genetic architecture (Bull, 2015). The morphological distinction between 2-row and 6-row phenotypes is determined by the fertility status of lateral spikelets. In 2-row barley, only central spikelets are fertile and develop grains, while lateral spikelets remain sterile. In contrast, 6-row barley exhibits fertility in both central and lateral spikelets, producing more grains per spike and significantly influencing yield component traits (Youssef et al., 2017) such as thousand kernel weight and kernel number.

The genetic architecture underlying this trait involves a network of co-regulated genes; however, there is still little information on the exact mechanism (Zwirek et al., 2019). While *VRS1* on chromosome 2H serves as the most downstream genetic component (Komatsuda et al., 2007), several other characterised genes regulate lateral spikelet fertility and overall spike morphology, including *VRS2* in 5H (Youssef et al., 2017), *VRS3* (syn. INTERMEDIUM-A) in 1H (Van Esse et al., 2017; Bull et al., 2017), *VRS4* (syn. INTERMEDIUM-E) in 3H (Koppolu et al., 2013; Koppolu et al., 2022), and *VRS5* (syn. INTERMEDIUM-C) in 4H (Ramsay et al., 2011). Contemporary 6-row barley cultivars typically contain natural recessive *vrs1* and *vrs5* alleles (Zwirek et al., 2019).

Limitations of standard GWAS approaches

Various GWAS methods remain the predominant method for QTL discovery and genetic architecture analysis but face significant challenges including spurious associations, large background noise, and limited power to explain complex trait variants (Wang and Xu, 2019).

358 Our study utilised a diverse barley panel with pronounced population structure, providing an
359 opportunity to evaluate different mapping approaches with a trait documented to have
360 intricate genetic control.

361 Despite the significant improvement of statistical methods in both FarmCPU and BLINK that
362 employ multi-locus genome scans (Liu et al., 2016; Huang et al., 2019; Wang and Zhang,
363 2021), these approaches only detected the major *VRS1* gene, failing to identify other known
364 genes associated with row-type characteristics (Table 1). This limitation exemplifies a
365 common problem in complex trait analysis where primary morphological characteristics are
366 influenced by secondary traits confounded by genetic background (Zwirek et al., 2019) or
367 masked due to epistatic interaction (Ramsay et al., 2011). The low detection power also likely
368 stems from uncompounded effects of co-regulated genetic interactions (Tam et al., 2019),
369 even after controlling for population structure. This can occur when the effect of a QTL is
370 split amongst multiple markers because of extensive LD (correlation) structures between the
371 markers and QTL. Alternatively, each of the multiple markers may only capture a part of the
372 QTL effect if they are only partially correlated with the QTL (Meuwissen and Goddard, 2000;
373 Marchini et al., 2004; Goddard, 2009; Zhang et al., 2010).

374 Notably, a critical constraint of GWAS is the reliance on stringent significance thresholds,
375 which are implemented to decrease false positives at the expense of decreasing power and
376 increasing the number of false negatives for variants with modest effects. The conventional
377 approach of applying genome-wide significance thresholds (FDR adjustments or Bonferroni-
378 corrected values) prioritizes certainty of associations over discovery breadth. This limits
379 statistical power, excluding true causal variants that fall below the significance threshold
380 (Wang et al., 2016; Tam et al., 2019). A recent alternative to Bonferroni and FDR adjustment
381 on all markers utilized the LD between markers to calculate the true number of effective tests
382 and control type I error (Gao et al., 2008). This would likely increase the power to detect
383 QTL and is based on a similar philosophy to haploblocking, but it would not necessarily
384 recover any split signal like the localGEBV method would. However, we employed a similar
385 approach in a GWAS framework to compute the orthogonal amount of information each
386 block contained to validate the use of haploblock variance as a useful metric in breeding and
387 QTL discovery independent of GWAS. Utilizing this same approach, we were able to
388 increase our power in a GWAS framework as evidenced by the detection of known QTL
389 (Table 1). As one might expect, the relationship between haploblock variance and p-value
390 was quite strong (Supplementary Figure 4), and our approach was able to identify the known

391 QTL despite Bonferroni and FDR p-value correction. Interestingly, the unadjusted p-value
392 distribution was heavily skewed towards 1 (Supplementary Figure 4) with a small increase
393 between 0 and 0.10. The skew towards 1 and small increase near 0 indicated our approach
394 was highly conservative compared to the expected uniform null p-value distribution while
395 also preserving blocks associated with known QTL.

396 In a trait where multiple genes contribute through intricate regulatory networks, like barley
397 row-type, the statistical stringency employed by classical GWAS methods disproportionately
398 penalize small-effect loci that collectively determine phenotypic expression for complex,
399 polygenic traits. This in turn leads to GWAS having low power to disentangle background
400 noise from true signal (e.g., Figure 4). This phenomenon has been well-documented across
401 multiple crop species. In maize, numerous small-effect loci controlling numerous phenotypic
402 traits were missed by conventional GWAS but enriched with synonymous SNP because of
403 linkage with nearby causal SNP (Wallace et al., 2014). In rice, chlorophyll content and stay-
404 green traits are governed by networks of interacting genes whose individual effects were too
405 small to reach significance thresholds yet collectively explained substantial phenotypic
406 variation (Zhao et al., 2019). Bustos-Korts et al. (2019) demonstrated that barley adaptation
407 traits, such as developmental and row-type traits, are controlled by complex networks of
408 interacting loci whose effects become diluted when analysed individually. However, these
409 effects can be captured by exomic haplotype states due to the larger number of allelic states,
410 supporting our observation that genetic interactions in the *VRS* gene network may go
411 undetected using conventional approaches.

412 **Methodological advantages of localGEBV**

413 In contrast to standard GWAS, the localGEBV approach demonstrated superior detection
414 power for known genes associated with barley spike row phenotype. This is because the
415 localGEBV haploblocking method prevents overcorrecting p-values as it accounts for non-
416 independency among markers, as previously discussed in GWAS limitations (similar to Gao
417 et al., 2008 methods). The localGEBV method also collates genomic signals that are truly
418 dispersed because of LD in small to moderate effect loci, which maximizes power and
419 simultaneously reduced background noise. This was especially true under the infinitesimal
420 assumptions of rrBLUP, which tended to disperse the signal (e.g., Supplementary Figure 2).
421 Thus, we likely controlled the number of false negatives by collating dispersed QTL signals
422 when accounting for LD structure and preventing the overcorrection of p-values. We

423 demonstrate this by showing that FarmCPU and BLINK detected only the major *VRS1* gene
424 on chromosome 2H, whereas the localGEBV approach additionally identified haploblocks
425 containing other known row-phenotype regulators. These included *VRS3* in 1H (Van Esse et
426 al., 2017; Bull et al., 2017), *VRS5* in 4H (Ramsay et al., 2011), and several annotated QTL
427 (Youssef et al., 2017) that remained undetected by conventional methods (Figure 4).

428 Notably, the localGEBV methods reduced the background noise compared to the GWAS
429 results from FarmCPU and BLINK, and clearly delineated genomic signals regardless of
430 whether marker effects were estimated using rrBLUP or BayesR. The smoothing of
431 background noise (e.g., Figure 4 comparing variance of localGEBV background to FarmCPU
432 and BLINK background) may be indicative of marker effects from non-QTL regions
433 averaging towards small values or additional shrinkage if the markers were non-informative.
434 The averaging and/or shrinkage would reduce the corresponding haploblock variance when
435 combined into localGEBV utilising LD structure. This demonstrates our method's ability to
436 leverage localised genomic information to capture QTL signals that would otherwise be lost
437 to background noise and false-positive control. Admittedly, the repressed background noise
438 was initially surprising, because haploblock variance would be expected to scale with the
439 number of markers in the block in a situation where all markers were independent. We
440 demonstrated this to not be the case in Figure 2 comparing number of markers to the
441 haploblock variance and by fitting a generalized additive model. This highlights that using
442 LD to define block structures counteracts this increase and was broadly successful in
443 reducing background noise.

444 In addition to greater detection power to known QTL, the localGEBV method leverages
445 localised information on LD to fine-tune the region of interest. This relies on historic
446 recombination, drift, and selection patterns that influenced the LD development in the
447 genomic region. In contrast, when interpreting GWAS results, there is no defined region of
448 interest and genome-wide average LD patterns are often utilised to investigate potential QTL
449 or genes of interest. Thus, our methodology helps to accurately assess where a QTL may
450 reside (Figure 3B). However, the choice in haploblock parameters clearly suggested there
451 may be a trade-off in QTL discovery compared to greater genomic resolution to precisely
452 map the QTL. Furthermore, if parameters are too stringent, the QTL may lie outside of the
453 haploblock region even if it is determined to be significant. This is because other markers
454 outside of the block may also be capturing QTL effects even if they are in lower LD with
455 other markers.

456 A key advantage of the localGEBV approach beyond statistical power and accurately
457 defining QTL regions is its flexibility in accommodating different genomic prediction models
458 to estimate haplotype effects, as exemplified in Figure 4 and 5B. BayesR demonstrated
459 exceptional precision in estimating large-effect QTL, particularly visible in the *VRS1* region.
460 This is not surprising as it aligns with the major role of *VRS1* in the development of the six-
461 rowed spike phenotype controlled by a single recessive allele (*vrs1*), in contrast to the
462 dominant allele for the two-rowed phenotype (Komatsuda et al., 2007). This advantage stems
463 from the model's ability to accommodate various assumptions in estimating marker effects
464 (Erbe et al., 2012; Moser et al., 2015; Wolc and Dekkers, 2022), leading to improved
465 genome-wide QTL discovery (Kemper et al., 2015; Van Den Berg et al., 2019; Xiang et al.,
466 2021). Conversely, rrBLUP showed advantages in detecting candidate regions with multiple
467 small-effect alleles that cumulatively form a significant signal (Figure 4, Supplementary
468 Figures 2 and 4) and is suggestive of greater applicability for most quantitative traits with
469 near-infinitesimal genetic architecture. However, these candidate regions could not be
470 explicitly verified, because they were not known QTL, and thus more work is needed to
471 determine if rrBLUP truly had greater power than BayesR for small to moderate effect QTL.
472 This model flexibility allows application without prior knowledge of the trait's genetic
473 architecture, making it suitable for diverse breeding scenarios. For instance, this is evident in
474 the nearby *VRS1* region, where rrBLUP captured higher variance blocks (2H:b000210; Figure
475 3, Supplementary Figure 2). This region was not found to co-locate with known genes or
476 QTL, suggesting it could represent a potentially new QTL associated with row-type and
477 requires further investigation to determine if it is a new QTL. Thus, our results indicate that
478 the localGEBV method can capture different distributions of marker effects by utilising the
479 infinitesimal assumptions found in rrBLUP.

480 **LD parameters and genetic implications**

481 The precision of QTL discovery using localGEBV is directly influenced by LD structure
482 within the population. Indirectly, it is also based on marker positions. While we had a high-
483 quality reference map, it may be prudent to ignore marker positions and use the LD patterns
484 (genetic map) to form haploblocks if the reference is poorly constructed. It is also worth
485 noting that we utilized genome-wide blocking parameters, but parameters can also be defined
486 at the chromosomal level.

Our analysis determined that while varying LD parameters affected haploblock size, they did not alter the detection of informative segments for large, known effects (e.g., Figure 3A). This finding aligns with previous studies concluding that no 'universal' or optimal haploblock construction method applied to breeding programs exists (Andrade et al., 2019; Difabachew et al., 2023; Weber et al., 2023). Stringent LD ($r^2 = 0.5$) produced smaller haploblocks (often comprised of a single marker) enabling fine mapping of specific genes, while relaxed LD ($r^2 = 0.1$) generated larger haploblocks (Figure 3) independent of the genomic prediction method. The ability to choose parameters allows for flexibility and balancing the trade-offs between detection proportion and fine-resolution mapping when conducting QTL discovery studies. This is a clear advantage not currently found in most, if not all, GWAS methods without utilising different priors on the underlying genetic architecture. In conjunction with likely lower power to detect low to moderate effect QTL based on our results, the area to search for QTL is often defined by genome-wide average LD patterns. The localGEBV method overcomes both challenges.

The biological significance of haploblock size warrants consideration. Smaller haploblocks may signify high LD between markers and the QTL (Andrade et al., 2019), which facilitates precise candidate gene identification for post-GWAS analysis (Clark, 2004). On the other hand, larger haploblocks likely capture important biological mechanisms including local epistasis, pleiotropy (Kouyos et al., 2007; Zhang et al., 2014; Jiang et al., 2018), and adaptive mechanisms from balancing selection, mutation, and genetic drift (Barton, 2010). We did not observe this in our case, but we utilised a genetically intricate trait rather than fully Mendelian with substantial non-additive effects between a low number of loci.

Additionally, information on recombination hotspots at haploblock boundaries (Kim et al., 2018; Epstein et al., 2023) can be valuable for breaking unfavourable linkage drag in breeding programs (Bohra et al., 2022) or stacking favourable haplotypes. Utilizing haploblocks provides an interesting advantage when introgressing new QTL (haplotypes) for a complex population structure. Utilising localGEBV from haploblocks provides a "genetic insurance policy" by co-selecting target genes with their local genetic background, thereby ensuring more predictable and stable trait expression when introgressed into new cohorts. The latter point is especially important in genetic improvement to maintain diversity and construct the “ultimate genotype” (Cole and VanRaden, 2011; Kemper et al., 2012; Hayes et al., 2024). The latter suggests our results likely have implications in breeding programs, crossing designs, and genomic improvement. This is comparable to GWAS and genomic

520 selection sharing the same underlying framework and considerations, so it is natural to extend
521 our framework and its implications to genomic improvement. In such a case, selection of
522 blocks based on the haploblock variance or utilising the number of blocks capturing a set
523 proportion of the genetic variation could be utilised in breeding applications.

524 Lastly, it is important to note that constructing haploblocks based on LD is not always
525 possible. When constrained by LD structures from diverse populations (Abdellaoui et al.,
526 2023) like those commonly found in diversity panels, when SNP density is not homogeneous
527 (Li et al., 2021), or when markers are extremely dense with common alleles mixed with rarer
528 alleles (Taliun et al., 2014), alternative haploblock construction methods such as sliding
529 window approaches (Weber et al., 2023), gene boundary-based collapsing methods (Dering et
530 al., 2011), or incremental haploblock partitioning (Taliun et al., 2014) could be more
531 advantageous. However, the implications of these methods to QTL detection in the
532 localGEBV framework has not yet been explored.

533 **Biological insights from localGEBV features**

534 The localGEBV approach provides deeper understanding of trait genetic architecture through
535 two key features:

536 *Haploblock variance*. Haploblocks with high variances (greater than the mean haploblock
537 variance) were consistently associated with substantial haplotype effects, representing true
538 biological signals rather than artifacts of segment size because size was not correlated with
539 variance (Figure 2 and 6). This variance metric offers advantages over conventional p-values
540 in GWAS, which provides statistical significance but often lack informative biological
541 meaning (Visscher et al., 2017), may suffer from false associations (Yang et al., 2010; Wray
542 et al., 2013) and do not provide a definitive region to explore QTL. In addition, GWAS may
543 also only capture part of the QTL signal or share its effect with nearby markers in high LD
544 with the QTL (Meuwissen and Goddard, 2000; Marchini et al., 2004; Goddard, 2009; Zhang
545 et al., 2010); however, this is dependent on the prior assumptions of marker effects, towards
546 which our approach is more robust. By shifting focus from marker significance thresholds to
547 haploblock variance or testing haploblock variance for significance, the localGEBV approach
548 diminishes the problems associated with multiple testing that also makes small-effect loci
549 effectively undetectable. The reduction in stringency is because there are often far less
550 haploblocks than markers, so less stringency on type I error control is needed. The reduction
551 in the number of tests is appropriate, because markers are not independent and Bonferroni or

FDR corrections assume test independence (Gao et al., 2008). Variance patterns can indicate a high degree of polymorphism in regions under selection pressure or fixation (Maynard and Haigh, 2007), absence of selective interactions (Otto and Barton, 1997), or enriched mutations affecting trait heritability (Sullivan et al., 2023).

Haplotype effects. Haplotypes provide superior predictive ability compared to single markers. Our regression analyses demonstrated that the haplotype configurations within a particular, high-variance haploblock serve as better predictors of phenotypic traits than individual SNP genotype configurations. This highlights the importance of considering cumulative genetic effects in tightly linked regions (Meuwissen and Goddard, 2000), rather than isolated markers as single markers can only capture a limited amount of genetic variation.

The choice of estimating SNP effects (Step 2) to calculate localGEBV provides flexibility of this approach. While BayesR was able to confirm known large effect *VRS1* region (Figure 3 and 7A; Supplementary Figure 2), complex traits will not have this type of architecture and rrBLUP or other similar infinitesimal models is a good default model.

Lower-frequency alleles with considerable effect can be successfully captured as a single unit within the haploblock (Berdan et al., 2023), enabling exploration of local allelic interactions and epistasis (Charlesworth, 1974). The localGEBV method may help to capture these rare effects, but only if there are QTL and markers that have similar frequencies because LD is dependent on similar allele frequencies.

Lastly, haplotype effects also signify directionality (Han and Pan, 2010) in relation to a reference haplotype, similar to the allele substitution effect of the alternative allele relative to the reference allele. Our analysis confirmed that negative-effect haplotypes were associated with 2-row phenotypes and positive-effect haplotypes with 6-row spikes (Figure 7A and 7D).

Limitations of localGEBV

The localGEBV method represents a promising leap forward from a single marker to LD-based haplotype approach. However, the implementation we present here is based solely on additive genetic effects and aggregating dispersed QTL signals using LD. Regarding the latter, this means that haploblocks are based on historic selection, drift, and recombination patterns that influence the development and decay of LD (Slatkin, 2008). However, if intense selection and drift were driving quick formation of LD, it could indicate that haploblock boundaries are not reflective of future recombination “hotspots.” In such a case, the

583 localGEBV are not representative of regions that will be inherited more often than expected,
584 but may still aggregate QTL effects dispersed across multiple, highly correlated markers (i.e.,
585 statistical advantages rather than biological interpretation). Thus, biological interpretation of
586 haploblock boundaries is determined on the specific population that is analysed, its
587 population structure, and recent selection history.

588 Furthermore, while only additive genetic effects are considered here, non-additive genetic
589 effects, such as dominance and epistasis, could be incorporated into the calculations to
590 compute local genomic estimated genotypic values (localGEGV) rather than localGEBV. It is
591 conceivable that dominance effects could be "solved" for individual loci much in the same
592 way additive marker effects are derived from Genomic Best Linear Unbiased Prediction
593 using dominance or genotypic value relationship matrices (e.g., Vitezica et al., 2017; Liu et
594 al., 2022). The local genomic estimated dominance deviation values for a haploblock would
595 then simply be the sum of the estimated dominance deviation values across the loci in the
596 block and the localGEGV the sum of local genomic estimated dominance deviation values
597 and localGEBV. Bayesian methodologies to directly compute dominance deviation and
598 genotypic values have similar interpretations to directly computing additive marker effects
599 using Bayesian alphabet methods (e.g., Wellmann and Bennewitz, 2012). Vitezica et al.
600 (2017) have similarly proposed methods to compute orthogonal epistasis effects, which
601 represents an opportunity to exploit epistatic interactions. However, how epistatic interaction
602 effects would be incorporated from epistatic relationship structures, or even a direct
603 interaction model (Bayesian or otherwise) remains an active area of exploration.

604 **Implications for crop breeding**

605 The localGEBV approach offers significant advantages in QTL discovery that could be used
606 in genetic improvement strategies in crops. By exploiting LD blocks, breeders can determine
607 both global and local genetic correlations between multiple traits (Visscher et al., 2017;
608 Olasege et al., 2022), identify sources of genetic control under pleiotropic influence
609 (Watanabe et al., 2019), and select favourable haplotype configurations. The approach
610 effectively identifies compound-effect loci (Bevan et al., 2017) that influences complex traits.
611 The approach is particularly valuable for traits that are difficult to phenotype; for example,
612 fertility in barley is difficult to phenotype because fertility of lateral spikelets drives row-type
613 morphology. Consequently, fertility can influence other yield components such as grain
614 number and thousand kernel weight.

615 As an example of a useful application, haploblocks that may benefit two unfavourably
616 correlated traits can be identified to guide parental selection and stack haplotypes that may
617 increase the rate of long-term genetic gain compared to utilising genome-wide GEBV. In
618 essence, precise parental combinations and mating pathways can be identified to ensure long-
619 term, consistent genetic gain in unfavourably correlated traits. This would be at odds with
620 multi-trait selection in traditional genomic prediction frameworks, because multi-trait
621 selection is expected to exhaust favourable genetic covariation between the traits, leaving
622 only neutral or unfavourable genetic covariation (Itoh, 1991). The latter would make genetic
623 progress for both traits increasingly more difficult over time (Itoh, 1991).

624 In practice, linkage drag between haplotypes pose a challenging task in breeding. Haplotype
625 boundaries signifying recombination hotspots can be broken down using targeted
626 recombination approach. On the other hand, for a more deployable application, localGEBV
627 information can be used to develop haplotype markers, especially for qualitative or
628 oligogenic traits such as disease resistance.

629 The ability to map haploblocks and identify specific haplotypes associated with traits
630 provides a powerful framework for unravelling genetic architecture that can be used to
631 advance crop breeding efforts. While we used a diverse germplasm with unique population
632 structure in this paper, the localGEBV method can also be applied in commercial breeding
633 populations or other experimental populations such as MAGIC or NAM, showing higher
634 detection ability (e.g., Varshney et al., 2021; Brunner et al., 2024; Tong et al., 2024; Akinlade
635 et al., 2025; Alahmad et al., 2025; Roy et al., 2025; Vo Van-Zivkovic et al., 2025; Aldiss et
636 al., 2025). These insights are essential for developing haplotype-based selection strategies
637 that assemble beneficial allele combinations and optimise genotype configurations (Hayes et
638 al., 2024), which would complement gene networks and genotype-to-phenotype systems
639 approaches (Cooper et al., 2009; Kemper et al., 2012; Villiers et al., 2024), and improve
640 genomic predictions (Schopp et al., 2017) in crop breeding programs.

641 To summarize the benefits to QTL discovery and breeding programs, the haploblock
642 approach represents an innovative compromise between GWAS and genomic selection,
643 combining the strengths of both methodologies while addressing their respective limitations.
644 While GWAS provides precise identification of QTL underlying traits of interest, its
645 applications remain largely confined to pre-breeding activities with limited direct utility for
646 practical breeding programs. Conversely, genomic selection effectively estimates genome-

wide breeding values for direct use by breeders but offers limited insights into the underlying genetic architecture of target traits and can severely impact diversity with intense selection. The localGEBV method bridges this gap by simultaneously enabling the dissection of genetic control mechanisms and the identification of genomically-informed selection units (haploblocks) directly applicable in breeding programs. The flexibility to adjust block size according to specific breeding objectives to reflect LD structures further enhances the practical utility of this approach, allowing breeders to optimize the balance between genetic resolution and selection efficiency. Such dual functionality positions haploblocks as a powerful tool for translating genomic discoveries into actionable breeding strategies.

Future research should explore extended genomic prediction models to capture rare variants, non-additive or epistatic interactions, leverage advancements in SNP arrays or whole genome sequencing to improve the haplotype blocking algorithm, haplotype phasing accurately, and explore the applications of localGEBV in selection under extensive genotype-by-environment interactions and multi-trait selection.

In conclusion, we demonstrated the localGEBV methodology is a powerful tool for QTL discovery. The localGEBV method was able to detect more known QTL with clearer signals compared to other GWAS methods. Furthermore, it alleviated or eliminated many of the limitations associated with multiple-testing, background noise, dependence on prior marker distribution (genetic architecture) assumptions, and defining regions of interest for candidate gene/QTL discovery based on significant associations. The localGEBV method was able to locate the largest effect QTL of interest with better prediction accuracy in a genomic selection context and was able to identify other known QTL as well as several putative QTL that FarmCPU and BLINK could not identify. When utilised in a genomic prediction or QTL context, the localGEBV method was robust to *a priori* assumptions of the genetic architecture, with near equivalent phenotypic prediction accuracy from a large effect QTL using an infinitesimal modelling approach or marker prior mixture approach to marker effects.

Methods

Barley phenotypic and genotypic datasets

We analysed $N = 812$ barley accessions with complete genotypic and spike row morphology data acquired from the AGG, representing global diversity originating from 80 countries.

Accessions were genotyped using the Illumina Infinium wheat-barley 40K XT SNP chip array (Keeble-Gagnère et al., 2021), yielding M = 12,539 SNP markers. Genotype calls were in 0/1/2 format (homozygous reference, heterozygous, homozygous alternate) relative to the cv Morex assembly IBSC v2.0.

Data filtering excluded unmapped markers and applied the following criteria using SelectionTools (Hofheinz and Frisch, 2014): >20% missing data, <1% expected heterozygosity, and <1% minor allele frequency. This resulted in M = 9,050 mapped markers for analysis. Accessions with >20% missing marker data were also excluded, leading to N = 790 accessions remaining.

Spike row descriptions obtained from AGG classified accessions as 2-rowed (373) or 6-rowed (384). For simplicity, we excluded 33 accessions that were described as 'irregular' row-type (Åberg and Wiebe, 1945), had missing information, or had 'mixed' designations. After exclusion of accessions with ambiguous designations, the dataset with row-type for QTL discovery analyses comprised N = 759 barley accessions. All analyses were performed using R version 3.6.3.

Population genetic structure and linkage disequilibrium analysis

We performed classical multidimensional scaling analysis of Roger's genetic distance using SelectionTools on the M = 9,050 mapped markers to infer population structure across the N = 790 barley accessions prior to filtering accessions for ambiguous row-type phenotypes. A *k-means* clustering algorithm categorised accessions into clusters, with the optimal number (*clusters* = 3) determined according to the majority of the criterion indices from the NbClust package (Charrad et al., 2014).

For linkage disequilibrium (LD) assessment, we calculated the squared pairwise correlations (r^2) between intrachromosomal SNP pairs. The LD decay was evaluated by analysing average r^2 between adjacent SNP as a function of physical distance, with positions aligned to the reference cv Morex assembly IBSC v2.0 as in the 40K XT SNP chip array.

QTL discovery approach

'Local' GEBV approach

The localGEBV approach consists of three key steps:

Step 1: Haploblock construction. Genome-wide markers were first organised into haploblocks using an LD-based approach (Supplementary Figure 5), which provides insight into physical recombination events. Due to its reduced dependence on allele frequencies and independence from finite population size, we used the squared correlation coefficient, r^2, as the LD measure following methodologies described by Voss-Fels et al. (2019).

Given the LD characteristics of our barley population, we tested multiple blocking criteria: $r^2 \in \{0.1, 0.3, 0.5\}$ and marker tolerances, $tol \in \{0, 1, 2, 3\}$, resulting in 12 LD blocking parameter combinations. The algorithm scanned each barley chromosome independently to group SNP markers into blocks based on the LD threshold and tolerance parameters. To make blocks, the r^2 measurement between the last marker in a block (or the first marker in a new block) and the adjacent marker was evaluated against the specified threshold to determine whether the marker would be included in the haploblock. If the r^2 value was below the threshold, the block would either be terminated, or the tolerance counter would be incremented by one. The marker tolerance parameter specified how many markers could fail the threshold check before a block was terminated. Specifying a tolerance greater than zero allows the algorithm to handle issues in the data sequencing, allele calls, or issues with the reference genome construction or reference alignment. A tolerance of 0 build would build haploblocks strictly based on pair-wise marker LD. A block may be composed of a single marker if it is not in LD with other markers, but is notably still considered a block. The algorithm continued until all markers were grouped into blocks.

Step 2. Estimation of SNP effects. We tested two models to estimate SNP effects for comparison: rrBLUP and BayesR. Following the approach described by Voss-Fels et al. (2019), the rrBLUP method was implemented in SelectionTools using:

$$\boldsymbol{y} = \boldsymbol{X\beta} + \boldsymbol{Zu} + \boldsymbol{e}, \qquad [1]$$

where $\boldsymbol{y}$ is the observation vector of N genotypes for row-type trait, $\boldsymbol{X}$ is the $N \times p$ design matrix allocating N phenotypes to p fixed effects, $\boldsymbol{\beta}$ is the size p vector of fixed effect solutions, $\boldsymbol{Z}$ is the $N \times M$ design matrix allocating phenotypes to the random effects of M SNP markers, $\boldsymbol{u}$ is the vector of M SNP effects, and $\boldsymbol{e}$ is the random residual errors. It is assumed that $\boldsymbol{u} \sim N(\boldsymbol{0_M}, \boldsymbol{I_M}\sigma_u^2)$ and $\boldsymbol{e} \sim N(\boldsymbol{0_N}, \boldsymbol{I_N}\sigma_e^2)$; where $\boldsymbol{0_M}$, σ_u^2, σ_e^2 , and $\boldsymbol{I}$ are a vector of zeros of length M, the additive genetic marker variance under infinitesimal assumptions, the residual variance, and identity matrices of size M and N, respectively. The rrBLUP solution for the M SNP marker effects, $\hat{\boldsymbol{u}}$ (Supplementary Figure 5), can be solved as:

$$\hat{\boldsymbol{u}} = (\boldsymbol{Z}'\boldsymbol{Z} + \lambda \boldsymbol{I}_{\boldsymbol{M}})^{-1}\boldsymbol{Z}'\boldsymbol{y}, \quad [2]$$

where $\lambda = \frac{\sigma_e^2}{\sigma_u^2}$, estimated in the rrBLUP software package, represents the ratio between the residual and SNP marker variances.

BayesR (Erbe et al., 2012; Moser et al., 2015) was implemented using GCTB v2.0 (Genome-wide Complex Trait Bayesian analysis, https://cnsgenomics.com/software/gctb) following the approach described by Kemper et al. (2015). The model was fit following the model in Equation 1 and used the same $\boldsymbol{Z}$ design matrix. However, BayesR assumes *a priori* that SNP effects, $\boldsymbol{u}$, are drawn from a mixture of K normal distributions with mean 0 and variances σ_k^2, with mixture probabilities defined by vector $\boldsymbol{\gamma} = [\gamma_1, \ldots, \gamma_K]$. At each iteration of the Gibbs sampler, the effect of SNP m is updated by first computing its posterior probabilities of membership in each mixture, conditional on the current effects of all other SNP and mixture probabilities in $\boldsymbol{\gamma}$. A component assignment b_m is then sampled from the posterior probabilities of membership to each mixture, and the SNP estimate, $\hat{u}_m$, is drawn from the corresponding normal distribution. After all SNP have been updated, the mixture proportions, $\boldsymbol{\gamma}$, are resampled from a Dirichlet distribution, with $\boldsymbol{\gamma} \sim \text{Dirichlet}(\boldsymbol{\alpha} + \boldsymbol{\delta})$, where $\boldsymbol{\alpha}$ is the vector of prior counts and $\boldsymbol{\delta}$ are the counts of SNP assigned to each of the K mixtures in an iteration of the Gibb's sampler.

In our implementation, we set $K = 4$ mixture components corresponding to zero-mean normal distributions with variance $\sigma_k^2 = \pi_k \sigma_g^2$, where $\boldsymbol{\pi} = [0, 0.0001, 0.001, 0.01]$ and σ_g^2 is the total additive genetic variance. The prior mixture probabilities were defined $\boldsymbol{\gamma} = [0.95, 0.03, 0.01, 0.01]$ and the prior counts were defined $\boldsymbol{\alpha} = \boldsymbol{1}_{\boldsymbol{K}}$, a vector of ones of length K. In other words, while the prior on an individual SNP effect distribution was informative, the prior on the overall genome-wide allocation to each mixture was left uninformative and the posterior was driven completely by the data. We ran 25,000 iterations of the Gibbs chain after 5,000 burn-in iterations.

Step 3. Estimation of localGEBV and variance. Linear contrasts of the estimated SNP effects were then specified to aggregate estimated SNP effects within each haploblock, yielding the estimated localGEBV of each individual at each haploblock (Kemper et al., 2015) as follows:

$$\boldsymbol{localGEBV_j} = \boldsymbol{Z_j}\hat{\boldsymbol{u}}_{\boldsymbol{j}}\,, \quad [3]$$

where $\boldsymbol{Z_j} = \boldsymbol{Z}_{\boldsymbol{m_r}:\boldsymbol{m_R}}$ is the design matrix of the marker genotypes (0/1/2 format for all N individuals) comprising haploblock j of J total haploblocks and $\hat{\boldsymbol{u}}_{\boldsymbol{j}} = \hat{\boldsymbol{u}}_{\boldsymbol{m_r}:\boldsymbol{m_R}}$ denotes the

767 vector of estimated SNP effects spanning from the first marker (m_r) to the last marker (m_R) in
768 haploblock *j* (Supplementary Figure 5). The $\boldsymbol{localGEBV_j}$ is the vector of *N* localGEBV values
769 at block j, similar to the vector of GEBV from a standard genomic selection model utilizing
770 the whole genome. Estimated SNP effects were obtained from Equation 2 in the rrBLUP
771 implementation or from the posteriors of the BayesR implementation of Equation 1 to compare
772 the two methods.

773 Subsequently, the variance of the estimated localGEBV effects (haploblock variance) across
774 individuals in haploblock *j* was defined to be:

$$\sigma^2_{haploblock_j} = var\left(\boldsymbol{localGEBV_j}\right) \quad [4]$$

775 where $\sigma^2_{haploblock_j}$ is the variance of the localGEBV at haploblock *j* and $\boldsymbol{localGEBV_j}$ is the
776 vector of *N* estimated localGEBV effects for all *N* individuals at block *j* (Supplementary
777 Figure 5). The variance represents the population variance calculation on the vector of
778 observed localGEBV values. In standard genomic prediction, $var(\boldsymbol{localGEBV_j})$ is
779 analogous to $var(\boldsymbol{GEBV})$ in the decomposition, $var(\boldsymbol{BV}) = var(\boldsymbol{GEBV}) + PEV(\boldsymbol{GEBV})$,
780 where $var(\boldsymbol{BV})$ is the variance of true BV, (i.e., the additive genetic variance in a genomic
781 BLUP, $\boldsymbol{G}\sigma^2_g$), $var(\boldsymbol{GEBV})$ is the variance of the estimated genomic BV captured by the data,
782 and $PEV(\boldsymbol{GEBV})$ is the prediction error variance of the estimated BV. Thus, the haploblock
783 variance represents the additive genomic variance attributable to a genomic segment that can
784 be captured by the data, rather than the total underlying genetic variance of the segment
785 (Mrode and Pocrnic, 2023). Here, we use the haploblock variance as a metric for prioritising
786 chromosome segments containing QTL. Haploblocks have previously been considered QTL
787 if the variance surpasses the overall mean haploblock variance (Kemper et al., 2015; Yadav et
788 al., 2025).

789 To assess whether high variance haploblocks were significantly different from zero, we
790 calculated probability values (p-values) using a chi-squared distribution with 1 degree of
791 freedom. The test statistic for a given block was as follows:

$$\chi^2_{haploblock_j} = \frac{df_j * \sigma^2_{haploblock_j}}{\sigma^2_{Null}} \quad [5]$$

792 where σ^2_{Null} was calculated by dividing the estimated additive genetic variance by the number
793 of blocks ($J = 1096$), indicating an infinitesimal assumption where variance is split equally
794 among blocks. The df was calculated as the effective number of markers in a block (i.e., the

795 independent and orthogonal pieces of information) by using eigen decomposition on the
796 genotype matrix of markers corresponding to block j. The number of eigenvalues that
797 explained at least 90% of the variation was considered the effective number of markers in the
798 block, similar to Gao et al. (2008). The resulting p-values were Bonferroni and FDR-
799 corrected and reported. The p-values were only generated for the set of LD parameters ($r^2 =$
800 0.1 and $tol = 3$) that maximized haploblock variance at the known *VRS1* locus.

801 To explore the relationship of haploblock variance with size and haplotype effects, a
802 generalized additive linear regression model, regressing haploblock variance on the number
803 of markers in the haploblock or the haplotype effect was performed using the R package
804 mgcv (Wood, 2001) to capture higher degree polynomial trends in the block variance and
805 block size relationship. Each of the 24 sets of LD blocks constructed from the combinations
806 of r^2 and tol parameters were analysed independently.

807 *Comparative genome-wide association studies and co-location analysis*

808 For comparative GWAS, we used the same genotype matrix in Equation 1 in two models
809 implemented in Genome Association and Prediction Integrated Tool (GAPIT) v3 in R (Wang
810 and Zhang, 2021): Fixed and random model Circulating Probability Unification (FarmCPU;
811 Liu et al., 2016) and Bayesian-information and Linkage-disequilibrium Iteratively Nested
812 Keyway (BLINK; Huang et al., 2019). FarmCPU iteratively incorporates fixed and random
813 effects, whereas BLINK uses only fixed effects. Unlike the standard single-locus mixed
814 linear model, which tests markers one at a time in a one-dimensional genome scan, both
815 FarmCPU and BLINK perform multi-dimensional genome scans that estimate multiple
816 marker effects simultaneously while controlling for population structure.

817 To account for population stratification, we fitted 15 principal components (explaining ~80%
818 cumulative variance) as covariates. To control for false discovery rate, significant markers
819 were identified following the built-in *P* value thresholds ($-\log_{10} P_{adj} > -\log_{10} 0.008$) for
820 FarmCPU and $-\log_{10} P_{adj} > -\log_{10} 0.004$) for BLINK).

821 Significant SNP markers identified by FarmCPU and BLINK were then compared with
822 haploblocks showing significant haploblock variance from rrBLUP and BayesR with co-
823 location. Co-location was based on the physical position according to the reference cv Morex
824 assembly IBSC v2.0 described in the 40K SNP chip array. We cross-referenced results with
825 known genes and QTL associated with row phenotypes, inflorescence development, fertility

826 of spikelets, overall spike morphology, and agronomic and yield component traits
827 (Komatsuda et al., 2007; Ramsay et al., 2011; Koppolu et al., 2013; Bull, 2015; Youssef et al.,
828 2017; Van Esse et al., 2017; Bull et al., 2017; Koppolu et al., 2022).

829 **Assessment of detecting true haploblocks**

830 First, to summarise the estimates of SNP effects obtained from FarmCPU, BLINK, rrBLUP,
831 and BayesR, we calculated their effect contributions in the principal components using the
832 factoextra (Kassambara and Mundt, 2016) R package.

833 To evaluate the accuracy of detecting a true QTL or haploblocks, we cross-validated the
834 population using an 80:20 split (training set of 589; testing set of 148) in a 5-fold scheme.
835 Detection accuracy, r, defined as the average from the 5-fold correlations between the
836 observed phenotypic values (y) and predicted values ($\hat{y}$) in the testing set. Specifically, we
837 tested the predicted effects of the haploblock with the highest variance identified by rrBLUP
838 and BayesR to predict the row-type phenotype compared to the most significant markers
839 identified by both FarmCPU and BLINK. This was done by fitting the discrete, categorical
840 haplotype configurations and discrete, categorical marker genotype configurations as fixed
841 effects in a LPM and in a logistic regression within a GLM framework in R. In the LPM,
842 estimation was performed by ordinary least squares, assuming the residual was normally,
843 independently, and identically distributed as an approximation because of the binary nature of
844 the row-type trait. In the logistic regression in the GLM framework, the same linear predictor
845 from the LPM was linked to the binomial distribution of the row-type trait via the logit link
846 function, thereby mapping the predictor to the probability scale.

847 For comparison, we repeated the analysis with random markers (i.e., non-significant) and
848 random haploblocks (i.e., with localGEBV variance below the threshold). Random selection
849 was repeated 100 times, and the mean correlation, r, and standard deviations (standard error
850 bars) of the 100 iterations were reported.

851 **Haplotype analysis**

852 To explore the two unique features of localGEBV (i.e., haploblock variance and haplotype
853 effects), we examined the specific haplotypes associated with the trait. As an illustrative
854 example, the haploblock with the highest variance was first subjected to statistical parsimony
855 haplotype network analysis (TCS method) implemented in POPART (Leigh et al., 2015).
856 Each haplotype, defined by a series of SNP alleles within the haploblock, was represented as

857 a node in the haplotype network. Using these haplotypes, we calculated pairwise similarity
858 scores based on the series of SNP alleles or haplotypes between accessions using FlapJack
859 (Milne et al., 2010) and subsequently performed complete linkage hierarchical clustering of
860 barley accessions. This enabled us to assess the relationship between haplotype similarity and
861 row-spike phenotypes.

Table 1. Summary statistics of high variance haploblocks for row-spike phenotype from localGEBV estimated using rrBLUP and BayesR, and significant markers identified using FarmCPU and BLINK. Only haploblocks with localGEBV Bonferroni or False Discovery Rate (FDR) corrected p-values are displayed.

Chr	Block ID	Flanking Marker[a]		Pos (Mbp)		Block Size[b]	Block Var*100		Bonferroni		FDR		GAPIT Method	GAPIT -log p-value
		Start	End	Start	End		rrBLUP	BayesR	rrBLUP	BayesR	rrBLUP	BayesR		
1H	b000049	AVRIG00513	AVRIG00594	352.32	387.55	50	0.264	0.333	1.80E-11	7.46E-15	5.99E-12	3.73E-15		
	b000055	AVRIG00645	AVRIG00696	404.23	413.96	43	0.079		6.80E-01		4.25E-02			
	b000056	AVRIG00697	AVRIG00741	414.06	428.36	34	0.093		2.12E-01		1.52E-02			
	b000067	AVRIG00854	AVRIG00900	459.03	474.21	37	0.067	0.058	1.16E-01	3.54E-01	1.16E-02	2.53E-02		
	b000075	AVRIG00950	AVRIG01001	492.4	503.66	38	0.071		7.25E-02		8.38E-03			
	b000091	AVRIG01071	AVRIG01107	516.8	520.21	32		0.112		1.61E-02		2.01E-03		
2H		AVRIG01687		44.79									BLINK	7.3
	b000210	AVRIG02156	AVRIG02455	231.42	431.25	137	0.577	0.263	1.11E-12	6.63E-05	5.57E-13	1.66E-05		
	b000214	AVRIG02569	AVRIG00273	496.67	550.02	116	0.262	0.111	4.52E-07	5.09E-02	9.04E-08	4.24E-03		
	b000235	AVRIG02998	AVRIG03058	645.1	655.33	49	0.817	1.33	3.37E-45	4.81E-74	3.37E-45	4.81E-74		
		AVRIG03038		651.38									FarmCPU	6
		AVRIG03040		651.53									BLINK	6.9
		AVRIG03047		652.42									FarmCPU, BLINK	17.6; 10.5
		1_1533		655.11									FarmCPU, BLINK	6.3; 5.8
3H	b000382	AVRIG04257	AVRIG04489	169.96	269.3	157	0.212	0.136	4.71E-08	1.47E-04	1.18E-08	2.45E-05		
	b000399	AVRIG04927	AVRIG05068	450.71	498.13	100	0.063	0.056	1.69E-02	4.87E-02	2.41E-03	4.24E-03		
	b000401	AVRIG05078	AVRIG05181	501.34	521.91	67	0.049		6.62E-01		4.25E-02			
	b000411	AVRIG05287	AVRIG05299	548.57	550.36	9		0.192		1.69E-01		1.30E-02		
4H	b000552	AVRIG06251	AVRIG06325	16.16	30.93	58	0.057	0.238	7.55E-02	3.86E-13	8.38E-03	1.29E-13		
		AVRIG06428		51.58									FarmCPU	7.05
	b000561	AVRIG06979	AVRIG06987	417.09	422.34	6		0.218		5.26E-01		3.50E-02		
	b000562	AVRIG06988	AVRIG07104	424.02	470.56	94	0.087		1.48E-01		1.23E-02			

	b000636	AVRIG07929	AVRIG07949	644.34	645.5	14		0.159		2.66E-02		2.73E-03		
5H	b000638	AVRIG07962	AVRIG08001	0.4	0.93	22		0.08		2.73E-02		2.73E-03		
	b000650	AVRIG08140	AVRIG08644	60.21	35.95	364	0.113	0.103	1.71E-03	5.07E-03	2.85E-04	7.24E-04		
6H	b000867	AVRIG10825	AVRIG10927	119	156.27	67	0.089		1.28E-01		1.17E-02			
7H	b001032	AVRIG13334	AVRIG13474	509.15	566.58	95	0.044	0.089	2.08E-01	1.25E-04	1.52E-02	2.45E-05		

[a] Markers within the haplotype blocks are presented as flanking markers; significant markers identified in FarmCPU and BLINK are shown.

[b] Block size corresponds to the number of markers within the defined haploblocks.

Funding

We thank the funding from the Grains Research and Development Corporation (UOQ2005-012RTX; Program 3. Minimising the impact of major barley foliar pathogens on yield and profit: Screening of diverse barley germplasm for rapid discovery and utilisation of novel disease resistance in barley using R-HapSelect – A haplotype-based toolkit).

Acknowledgements

We acknowledge Dr Sally Norton and the team at the Australian Grains Genebank for facilitating the acquisition of barley germplasm collection associated accession information; Dr Kerrie Forrest and the team at Agriculture Victoria for genotyping using the 40K Infinium XT SNP Chip; Dr Michael Groszmann at GRDC for discussions on the practical applications of localGEBV method. ED was supported by the Queensland Government's Industry Research Fellowships Program. LTH was supported through an ARC Future Fellowship (FT220100350). WS and VP were supported as Adjunct Postdocs of the Australian Research Council Training Centre in Predictive Breeding for Agricultural Futures (IC230100016).

Declaration of Interest

Lee T. Hickey is a member of the Plant Communications advisory board.

Author contributions

Conceptualization, E.D., K.V., L.H., and B.H.; data analysis and writing – review and editing, W.S., E.D., V.P., and S.Y.; Funding acquisition, E.D. All authors have read and approved the final manuscript.

Pre-Print Server

The article was submitted to the pre-print server, bioRxiv

DOI: https://doi.org/10.1101/2025.08.28.672830

References

Abdellaoui, A., Yengo, L., Verweij, K. J. H., and Visscher, P. M. (2023). 15 years of GWAS discovery: Realizing the promise. *Am. J. Hum. Genet.* **110**:179–194.

Åberg, E., and Wiebe, G. A. (1945). Irregular barley, Hordeum irregulare, sp. nov. *J. Wash. Acad. Sci.* **35**:161–164.

Akinlade, O. J., Robinson, H., Kang, Y., Thudi, M., Samineni, S., Gaur, P., Smith, M. R., Voss-Fels, K. P., Costilla, R., Varshney, R. K., et al. (2025). A chickpea MAGIC population to dissect the genetics of complex traits. *Plant Genome* **18**:e70096.

Alahmad, S., Smith, D., Katsikis, C., Aldiss, Z., Brunner, S. M., Meer, S. V., Meijer, L., Heidariask, B., Chenu, K., and Chapman, S. (2025). Phenotyping the hidden half: Combining UAV phenotyping and machine learning to predict barley root traits in the field. *J. Exp. Bot.* Advance Access published 2025.

Aldiss, Z., Lam, Y., Baraibar, S., Van Der Meer, S., Dinglasan, E., Massel, K., Crisp, P., Godwin, I., Borrell, A., Moody, D., et al. (2025). Haplotype-based insights into seminal root angle in barley. *Plant Genome* **18**:e70088.

Andrade, A. C. B., Viana, J. M. S., Pereira, H. D., Pinto, V. B., and Fonseca E Silva, F. (2019). Linkage disequilibrium and haplotype block patterns in popcorn populations. *PLOS ONE* **14**:e0219417.

Barton, N. H. (2010). Mutation and the evolution of recombination. *Philos. Trans. R. Soc. B Biol. Sci.* **365**:1281–1294.

Berdan, E. L., Barton, N. H., Butlin, R., Charlesworth, B., Faria, R., Fragata, I., Gilbert, K. J., Jay, P., Kapun, M., Lotterhos, K. E., et al. (2023). How chromosomal inversions reorient the evolutionary process. *J. Evol. Biol.* **36**:1761–1782.

Bevan, M. W., Uauy, C., Wulff, B. B. H., Zhou, J., Krasileva, K., and Clark, M. D. (2017). Genomic innovation for crop improvement. *Nature* **543**:346–354.

Bohra, A., Kilian, B., Sivasankar, S., Caccamo, M., Mba, C., McCouch, S. R., and Varshney, R. K. (2022). Reap the crop wild relatives for breeding future crops. *Trends Biotechnol.* **40**:412–431.

Brunner, S. M., Dinglasan, E., Baraibar, S., Alahmad, S., Katsikis, C., Van Der Meer, S., Godoy, J., Moody, D., Smith, M., Hickey, L., et al. (2024). Characterizing stay-green in barley across diverse environments: unveiling novel haplotypes. *Theor. Appl. Genet.* **137**:120.

Bull, H. J. (2015). Identification and Characterisation of the Barley Row-Type Gene VRS3 Advance Access published 2015.

Bull, H., Casao, M. C., Zwirek, M., Flavell, A. J., Thomas, W. T. B., Guo, W., Zhang, R., Rapazote-Flores, P., Kyriakidis, S., Russell, J., et al. (2017). Barley SIX-ROWED SPIKE3 encodes a putative Jumonji C-type H3K9me2/me3 demethylase that represses lateral spikelet fertility. *Nat. Commun.* **8**:936.

Bustos-Korts, D., Dawson, I. K., Russell, J., Tondelli, A., Guerra, D., Ferrandi, C., Strozzi, F., Nicolazzi, E. L., Molnar-Lang, M., Ozkan, H., et al. (2019). Exome

sequences and multi-environment field trials elucidate the genetic basis of adaptation in barley. *Plant J.* **99**:1172–1191.

Charlesworth, B. (1974). Inversion polymorphism in a two-locus genetic system. *Genet. Res.* **23**:259–280.

Charrad, M., Ghazzali, N., Boiteau, V., and Niknafs, A. (2014). **NbClust** : An *R* Package for Determining the Relevant Number of Clusters in a Data Set. *J. Stat. Softw.* **61**.

Clark, A. G. (2004). The role of haplotypes in candidate gene studies. *Genet. Epidemiol.* **27**:321–333.

Cole, J. B., and VanRaden, P. M. (2011). Use of haplotypes to estimate Mendelian sampling effects and selection limits. *J. Anim. Breed. Genet.* **128**:446–455.

Comadran, J., Ramsay, L., MacKenzie, K., Hayes, P., Close, T. J., Muehlbauer, G., Stein, N., and Waugh, R. (2011). Patterns of polymorphism and linkage disequilibrium in cultivated barley. *Theor. Appl. Genet.* **122**:523–531.

Cooper, M., Van Eeuwijk, F. A., Hammer, G. L., Podlich, D. W., and Messina, C. (2009). Modeling QTL for complex traits: detection and context for plant breeding. *Curr. Opin. Plant Biol.* **12**:231–240.

Dering, C., Hemmelmann, C., Pugh, E., and Ziegler, A. (2011). Statistical analysis of rare sequence variants: an overview of collapsing methods. *Genet. Epidemiol.* **35**.

Difabachew, Y. F., Frisch, M., Langstroff, A. L., Stahl, A., Wittkop, B., Snowdon, R. J., Koch, M., Kirchhoff, M., Cselényi, L., Wolf, M., et al. (2023). Genomic prediction with haplotype blocks in wheat. *Front. Plant Sci.* **14**:1168547.

Epstein, R., Sajai, N., Zelkowski, M., Zhou, A., Robbins, K. R., and Pawlowski, W. P. (2023). Exploring impact of recombination landscapes on breeding outcomes. *Proc. Natl. Acad. Sci.* **120**:e2205785119.

Erbe, M., Hayes, B. J., Matukumalli, L. K., Goswami, S., Bowman, P. J., Reich, C. M., Mason, B. A., and Goddard, M. E. (2012). Improving accuracy of genomic predictions within and between dairy cattle breeds with imputed high-density single nucleotide polymorphism panels. *J. Dairy Sci.* **95**:4114–4129.

Fan, B., Onteru, S. K., Du, Z.-Q., Garrick, D. J., Stalder, K. J., and Rothschild, M. F. (2011). Genome-Wide Association Study Identifies Loci for Body Composition and Structural Soundness Traits in Pigs. *PLoS ONE* **6**:e14726.

Gao, X., Starmer, J., and Martin, E. R. (2008). A multiple testing correction method for genetic association studies using correlated single nucleotide polymorphisms. *Genet. Epidemiol.* **32**:361–369.

Goddard, M. (2009). Genomic selection: prediction of accuracy and maximisation of long term response. *Genetica* **136**:245–257.

Han, F., and Pan, W. (2010). A Data-Adaptive Sum Test for Disease Association with Multiple Common or Rare Variants. *Hum. Hered.* **70**:42–54.

Hayes, B. (2013). Overview of Statistical Methods for Genome-Wide Association Studies (GWAS). In *Genome-Wide Association Studies and Genomic Prediction* (ed. Gondro, C.), Van Der Werf, J.), and Hayes, B.), pp. 149–169. Totowa, NJ: Humana Press.

Hayes, B. J., Mahony, T. J., Villiers, K., Warburton, C., Kemper, K. E., Dinglasan, E., Robinson, H., Powell, O., Voss-Fels, K., and Godwin, I. D. (2024). Potential approaches to create ultimate genotypes in crops and livestock. *Nat. Genet.* **56**:2310–2317.

Hofheinz, N., and Frisch, M. (2014). Heteroscedastic Ridge Regression Approaches for Genome-Wide Prediction With a Focus on Computational Efficiency and Accurate Effect Estimation. *G3 GenesGenomesGenetics* **4**:539–546.

Huang, M., Liu, X., Zhou, Y., Summers, R. M., and Zhang, Z. (2019). BLINK: a package for the next level of genome-wide association studies with both individuals and markers in the millions. *GigaScience* **8**:giy154.

Itoh, Y. (1991). Changes in genetic correlations by index selection. *Genet. Sel. Evol.* **23**:301–308.

Jiang, Y., Schmidt, R. H., and Reif, J. C. (2018). Haplotype-Based Genome-Wide Prediction Models Exploit Local Epistatic Interactions Among Markers. *G3 GenesGenomesGenetics* **8**:1687–1699.

Joukhadar, R., Daetwyler, H. D., Bansal, U. K., Gendall, A. R., and Hayden, M. J. (2017). Genetic Diversity, Population Structure and Ancestral Origin of Australian Wheat. *Front. Plant Sci.* **8**:2115.

Kassambara, A., and Mundt, F. (2016). Factoextra: extract and visualize the results of multivariate data analyses. *CRAN Contrib. Packag.* Advance Access published 2016.

Keeble-Gagnère, G., Pasam, R., Forrest, K. L., Wong, D., Robinson, H., Godoy, J., Rattey, A., Moody, D., Mullan, D., Walmsley, T., et al. (2021). Novel Design of Imputation-Enabled SNP Arrays for Breeding and Research Applications Supporting Multi-Species Hybridization. *Front. Plant Sci.* **12**:756877.

Kemper, K. E., Bowman, P. J., Pryce, J. E., Hayes, B. J., and Goddard, M. E. (2012). Long-term selection strategies for complex traits using high-density genetic markers. *J. Dairy Sci.* **95**:4646–4656.

Kemper, K. E., Reich, C. M., Bowman, P. J., Vander Jagt, C. J., Chamberlain, A. J., Mason, B. A., Hayes, B. J., and Goddard, M. E. (2015). Improved precision of QTL mapping using a nonlinear Bayesian method in a multi-breed population leads to greater accuracy of across-breed genomic predictions. *Genet. Sel. Evol.* **47**:29.

Kim, S. A., Cho, C.-S., Kim, S.-R., Bull, S. B., and Yoo, Y. J. (2018). A new haplotype block detection method for dense genome sequencing data based on interval graph modeling of clusters of highly correlated SNPs. *Bioinformatics* **34**:388–397.

Komatsuda, T., Pourkheirandish, M., He, C., Azhaguvel, P., Kanamori, H., Perovic, D., Stein, N., Graner, A., Wicker, T., Tagiri, A., et al. (2007). Six-rowed barley originated from a mutation in a homeodomain-leucine zipper I-class homeobox gene. *Proc. Natl. Acad. Sci.* **104**:1424–1429.

Koppolu, R., Anwar, N., Sakuma, S., Tagiri, A., Lundqvist, U., Pourkheirandish, M., Rutten, T., Seiler, C., Himmelbach, A., Ariyadasa, R., et al. (2013). *Six-rowed spike4* (*Vrs4*) controls spikelet determinacy and row-type in barley. *Proc. Natl. Acad. Sci.* **110**:13198–13203.

Koppolu, R., Jiang, G., Milner, S. G., Muqaddasi, Q. H., Rutten, T., Himmelbach, A., Guo, Y., Stein, N., Mascher, M., and Schnurbusch, T. (2022). The barley mutant multiflorus2.b reveals quantitative genetic variation for new spikelet architecture. *Theor. Appl. Genet.* **135**:571–590.

Kouyos, R. D., Silander, O. K., and Bonhoeffer, S. (2007). Epistasis between deleterious mutations and the evolution of recombination. *Trends Ecol. Evol.* **22**:308–315.

Leigh, J. W., Bryant, D., and Nakagawa, S. (2015). POPART: full-feature software for haplotype network construction. *Methods Ecol. Evol.* **6**.

Li, J., Wang, Z., Fernando, R., and Cheng, H. (2021). Tests of association based on genomic windows can lead to spurious associations when using genotype panels with heterogeneous SNP densities. *Genet. Sel. Evol.* **53**:45.

Liu, X., Huang, M., Fan, B., Buckler, E. S., and Zhang, Z. (2016). Iterative Usage of Fixed and Random Effect Models for Powerful and Efficient Genome-Wide Association Studies. *PLOS Genet.* **12**:e1005767.

Liu, T., Luo, C., Ma, J., Wang, Y., Shu, D., Qu, H., and Su, G. (2022). Including dominance effects in the prediction model through locus-specific weights on heterozygous genotypes can greatly improve genomic predictive abilities. *Heredity* **128**:154–158.

Marchini, J., Cardon, L. R., Phillips, M. S., and Donnelly, P. (2004). The effects of human population structure on large genetic association studies. *Nat. Genet.* **36**:512–517.

Maynard, J., and Haigh, J. (2007). The hitch-hiking effect of a favourable gene. *Genet. Res.* **89**:391–403.

Meuwissen, T. H. E., and Goddard, M. E. (2000). Fine Mapping of Quantitative Trait Loci Using Linkage Disequilibria With Closely Linked Marker Loci. *Genetics* **155**:421–430.

Meuwissen, T. H. E., Hayes, B. J., and Goddard, M. E. (2001). Prediction of Total Genetic Value Using Genome-Wide Dense Marker Maps. *Genetics* **157**:1819–1829.

Milne, I., Shaw, P., Stephen, G., Bayer, M., Cardle, L., Thomas, W. T. B., Flavell, A. J., and Marshall, D. (2010). Flapjack—graphical genotype visualization. *Bioinformatics* **26**:3133–3134.

Moser, G., Lee, S. H., Hayes, B. J., Goddard, M. E., Wray, N. R., and Visscher, P. M. (2015). Simultaneous Discovery, Estimation and Prediction Analysis of Complex Traits Using a Bayesian Mixture Model. *PLOS Genet.* **11**:e1004969.

Mrode, R., and Pocrnic, I. (2023). *Linear Models for the Prediction of the Genetic Merit of Animals*. 4th Edition. Boston, MA: CABI.

Olasege, B. S., Porto-Neto, L. R., Tahir, M. S., Gouveia, G. C., Cánovas, A., Hayes, B. J., and Fortes, M. R. S. (2022). Correlation scan: identifying genomic regions that affect genetic correlations applied to fertility traits. *BMC Genomics* **23**:684.

Otto, S. P., and Barton, N. H. (1997). The Evolution of Recombination: Removing the Limits to Natural Selection. *Genetics* **147**:879–906.

Ramsay, L., Comadran, J., Druka, A., Marshall, D. F., Thomas, W. T. B., Macaulay, M., MacKenzie, K., Simpson, C., Fuller, J., Bonar, N., et al. (2011). INTERMEDIUM-C, a modifier of lateral spikelet fertility in barley, is an ortholog of the maize domestication gene TEOSINTE BRANCHED 1. *Nat. Genet.* **43**:169–172.

Roy, D., Dinglasan, E., Fowler, R., Platz, G., Lance, R., Synman, L., Franckowiak, J., Hickey, L. T., Voss-Fels, K., and Robinson, H. (2025). Genomic regions associated with spot blotch resistance in elite barley breeding populations. *Mol. Breed.* **45**:16.

Schopp, P., Müller, D., Wientjes, Y. C., and Melchinger, A. E. (2017). Genomic prediction within and across biparental families: means and variances of prediction accuracy and usefulness of deterministic equations. *G3 Genes Genomes Genet.* **7**:3571–3586.

Slatkin, M. (2008). Linkage disequilibrium—understanding the evolutionary past and mapping the medical future. *Nat. Rev. Genet.* **9**:477–485.

Sullivan, P. F., Meadows, J. R. S., Gazal, S., Phan, B. N., Li, X., Genereux, D. P., Dong, M. X., Bianchi, M., Andrews, G., Sakthikumar, S., et al. (2023). Leveraging base-pair mammalian constraint to understand genetic variation and human disease. *Science* **380**:eabn2937.

Taliun, D., Gamper, J., and Pattaro, C. (2014). Efficient haplotype block recognition of very long and dense genetic sequences. *BMC Bioinformatics* **15**:10.

Tam, V., Patel, N., Turcotte, M., Bossé, Y., Paré, G., and Meyre, D. (2019). Benefits and limitations of genome-wide association studies. *Nat. Rev. Genet.* **20**:467–484.

Templeton, A. R., Crandall, K. A., and Sing, C. F. (1992). A cladistic analysis of phenotypic associations with haplotypes inferred from restriction endonuclease mapping and DNA sequence data. III. Cladogram estimation. *Genetics* **132**:619–633.

The Bovine HapMap Consortium, Gibbs, R. A., Taylor, J. F., Van Tassell, C. P., Barendse, W., Eversole, K. A., Gill, C. A., Green, R. D., Hamernik, D. L., Kappes, S. M., et al. (2009). Genome-Wide Survey of SNP Variation Uncovers the Genetic Structure of Cattle Breeds. *Science* **324**:528–532.

Tong, J., Tarekegn, Z. T., Jambuthenne, D., Alahmad, S., Periyannan, S., Hickey, L., Dinglasan, E., and Hayes, B. (2024). Stacking beneficial haplotypes from the Vavilov wheat collection to accelerate breeding for multiple disease resistance. *Theor. Appl. Genet.* **137**:274.

Van Den Berg, I., Hayes, B. J., Chamberlain, A. J., and Goddard, M. E. (2019). Overlap between eQTL and QTL associated with production traits and fertility in dairy cattle. *BMC Genomics* **20**:291.

Van Esse, G. W., Walla, A., Finke, A., Koornneef, M., Pecinka, A., and Von Korff, M. (2017). Six-Rowed Spike3 (VRS3) Is a Histone Demethylase That Controls Lateral Spikelet Development in Barley. *Plant Physiol.* **174**:2397–2408.

Varshney, R. K., Roorkiwal, M., Sun, S., Bajaj, P., Chitikineni, A., Thudi, M., Singh, N. P., Du, X., Upadhyaya, H. D., and Khan, A. W. (2021). A chickpea genetic variation map based on the sequencing of 3,366 genomes. *Nature* **599**:622–627.

Villiers, K., Voss-Fels, K. P., Dinglasan, E., Jacobs, B., Hickey, L., and Hayes, B. J. (2024). Evolutionary computing to assemble standing genetic diversity and achieve long-term genetic gain. *Plant Genome* **17**:e20467.

Visscher, P. M., Wray, N. R., Zhang, Q., Sklar, P., McCarthy, M. I., Brown, M. A., and Yang, J. (2017). 10 Years of GWAS Discovery: Biology, Function, and Translation. *Am. J. Hum. Genet.* **101**:5–22.

Vitezica, Z. G., Legarra, A., Toro, M. A., and Varona, L. (2017). Orthogonal estimates of variances for additive, dominance, and epistatic effects in populations. *Genetics* **206**:1297–1307.

Vo Van-Zivkovic, N., Dinglasan, E., Tong, J., Watt, C., Goody, J., Mullan, D., Hickey, L., and Robinson, H. (2025). A large-scale multi-environment study dissecting adult-plant resistance haplotypes for stripe rust resistance in Australian wheat breeding populations. *Theor. Appl. Genet.* **138**:72.

Voss-Fels, K. P., Stahl, A., Wittkop, B., Lichthardt, C., Nagler, S., Rose, T., Chen, T.-W., Zetzsche, H., Seddig, S., and Majid Baig, M. (2019). Breeding improves wheat productivity under contrasting agrochemical input levels. *Nat. Plants* **5**:706–714.

Wallace, J. G., Bradbury, P. J., Zhang, N., Gibon, Y., Stitt, M., and Buckler, E. S. (2014). Association Mapping across Numerous Traits Reveals Patterns of Functional Variation in Maize. *PLoS Genet.* **10**:e1004845.

Wang, M., and Xu, S. (2019). Statistical power in genome-wide association studies and quantitative trait locus mapping. *Heredity* **123**:287–306.

Wang, J., and Zhang, Z. (2021). GAPIT version 3: boosting power and accuracy for genomic association and prediction. *Genomics Proteomics Bioinformatics* **19**:629–640.

Wang, T., Chen, Y.-P. P., Bowman, P. J., Goddard, M. E., and Hayes, B. J. (2016). A hybrid expectation maximisation and MCMC sampling algorithm to implement Bayesian mixture model based genomic prediction and QTL mapping. *BMC Genomics* **17**:744.

Watanabe, K., Stringer, S., Frei, O., Umićević Mirkov, M., De Leeuw, C., Polderman, T. J. C., Van Der Sluis, S., Andreassen, O. A., Neale, B. M., and Posthuma, D. (2019). A global overview of pleiotropy and genetic architecture in complex traits. *Nat. Genet.* **51**:1339–1348.

Weber, S. E., Frisch, M., Snowdon, R. J., and Voss-Fels, K. P. (2023). Haplotype blocks for genomic prediction: a comparative evaluation in multiple crop datasets. *Front. Plant Sci.* **14**:1217589.

Wei, Z., Sun, W., Wang, K., and Hakonarson, H. (2009). Multiple testing in genome-wide association studies via hidden Markov models. *Bioinformatics* **25**:2802–2808.

Wellmann, R., and Bennewitz, J. (2012). Bayesian models with dominance effects for genomic evaluation of quantitative traits. *Genet. Res.* **94**:21–37.

Wolc, A., and Dekkers, J. C. M. (2022). Application of Bayesian genomic prediction methods to genome-wide association analyses. *Genet. Sel. Evol.* **54**:31.

Wood, S. N. (2001). mgcv: GAMs and generalized ridge regression for R. *R News* **1**:20–25.

Wray, N. R., Yang, J., Hayes, B. J., Price, A. L., Goddard, M. E., and Visscher, P. M. (2013). Pitfalls of predicting complex traits from SNPs. *Nat. Rev. Genet.* **14**:507–515.

Xiang, R., MacLeod, I. M., Daetwyler, H. D., De Jong, G., O'Connor, E., Schrooten, C., Chamberlain, A. J., and Goddard, M. E. (2021). Genome-wide fine-mapping identifies pleiotropic and functional variants that predict many traits across global cattle populations. *Nat. Commun.* **12**:860.

Yadav, S., Dillon, S., McNeil, M., Dinglasan, E., Jambuthenne, D., Mago, R., Dodds, P. N., Hickey, L. T., and Hayes, B. J. (2025). Advancing rust resistance in elite wheat with haplotype mapping and a novel introgression strategy. *bioRxiv* Advance Access published 2025.

Yang, J., Benyamin, B., McEvoy, B. P., Gordon, S., Henders, A. K., Nyholt, D. R., Madden, P. A., Heath, A. C., Martin, N. G., Montgomery, G. W., et al. (2010). Common SNPs explain a large proportion of the heritability for human height. *Nat. Genet.* **42**:565–569.

Yang, J., Zaitlen, N. A., Goddard, M. E., Visscher, P. M., and Price, A. L. (2014). Advantages and pitfalls in the application of mixed-model association methods. *Nat. Genet.* **46**:100–106.

Youssef, H. M., Eggert, K., Koppolu, R., Alqudah, A. M., Poursarebani, N., Fazeli, A., Sakuma, S., Tagiri, A., Rutten, T., Govind, G., et al. (2017). VRS2 regulates hormone-mediated inflorescence patterning in barley. *Nat. Genet.* **49**:157–161.

Youssef, H. M., Allam, M., Boussora, F., Himmelbach, A., Milner, S. G., Mascher, M., and Schnurbusch, T. (2020). Dissecting the Genetic Basis of Lateral and Central Spikelet Development and Grain Traits in Intermedium-Spike Barley (Hordeum vulgare Convar. Intermedium). *Plants* **9**:1655.

Zhang, Z., Ersoz, E., Lai, C.-Q., Todhunter, R. J., Tiwari, H. K., Gore, M. A., Bradbury, P. J., Yu, J., Arnett, D. K., and Ordovas, J. M. (2010). Mixed linear model approach adapted for genome-wide association studies. *Nat. Genet.* **42**:355–360.

Zhang, Z., Wang, W., and Valdar, W. (2014). Bayesian Modeling of Haplotype Effects in Multiparent Populations. *Genetics* **198**:139–156.

Zhao, Y., Qiang, C., Wang, X., Chen, Y., Deng, J., Jiang, C., Sun, X., Chen, H., Li, J., Piao, W., et al. (2019). New alleles for chlorophyll content and stay-green traits revealed by a genome wide association study in rice (Oryza sativa). *Sci. Rep.* **9**:2541.

Zwirek, M., Waugh, R., and McKim, S. M. (2019). Interaction between row-type genes in barley controls meristem determinacy and reveals novel routes to improved grain. *New Phytol.* **221**:1950–1965.

Supplementary Files

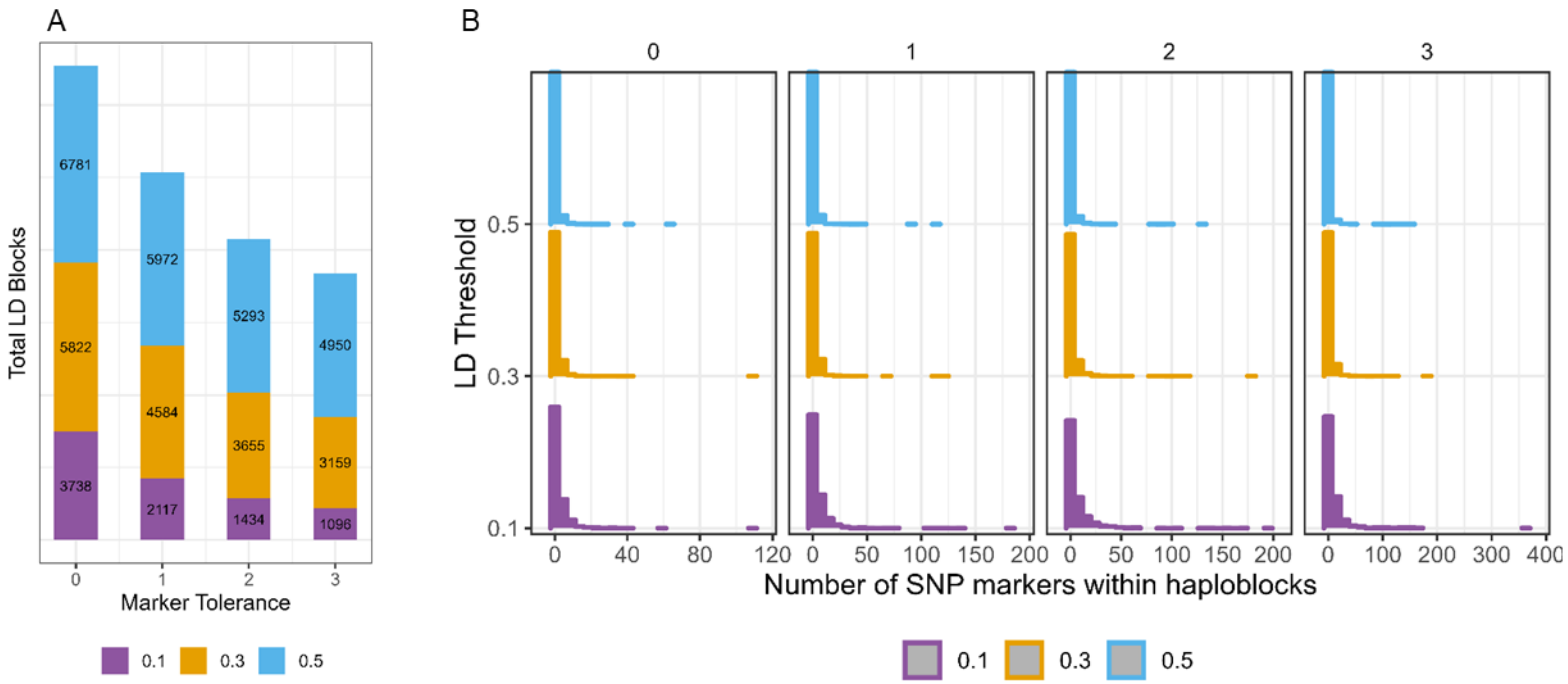

Supplementary Figure 1. LD block construction and its relationship with block size. SNP markers are grouped according to intrachromosomal pairwise LD based on the different LD-blocking parameters (LD threshold $r^2 \in \{0.1,0.3,0.5\}$; and marker $tol \in \{0,1,2,3\}$). (**A**) The number of total blocks for each combination of marker tolerance (x-axis) and LD threshold (colours and y-axis) are presented. (**B**) The distribution of the number of markers in each block for each combination of marker tolerance (x-axis) and LD threshold (colours and y-axis) are presented.

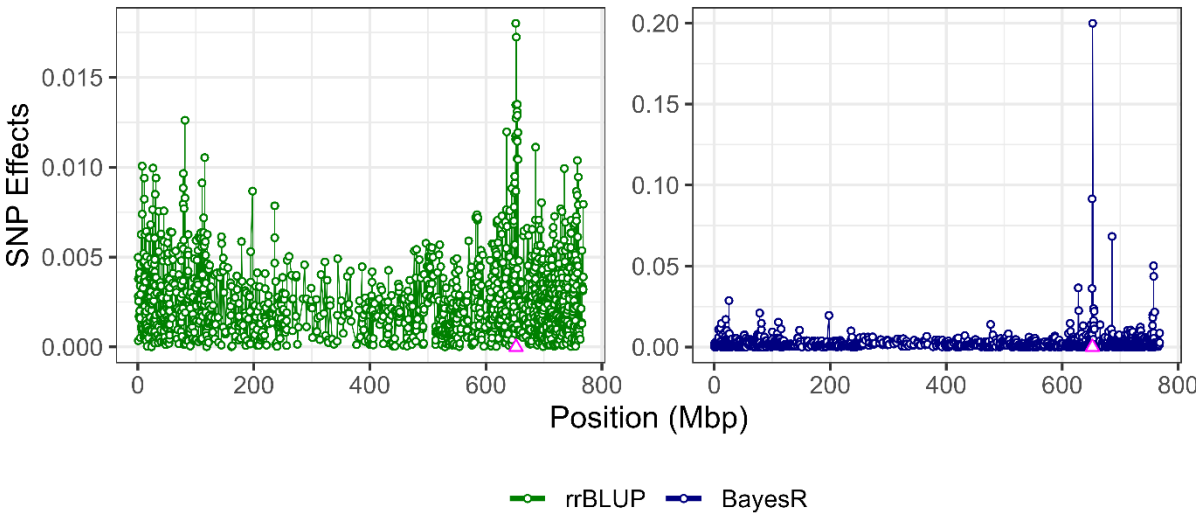

1180

1181 **Supplementary Figure 2. SNP effects estimated by rrBLUP and BayesR for row-type**
1182 **spike architecture in chromosome 2H.** Shown is the absolute value of SNP effect estimates,
1183 note the change of *y-axis* scale for rrBLUP and BayesR. The *VRS1* gene (marked as Δ) is
1184 located at 652.03 Mbp based on the XT SNP chip physical position using cv Morex assembly
1185 v2

1186

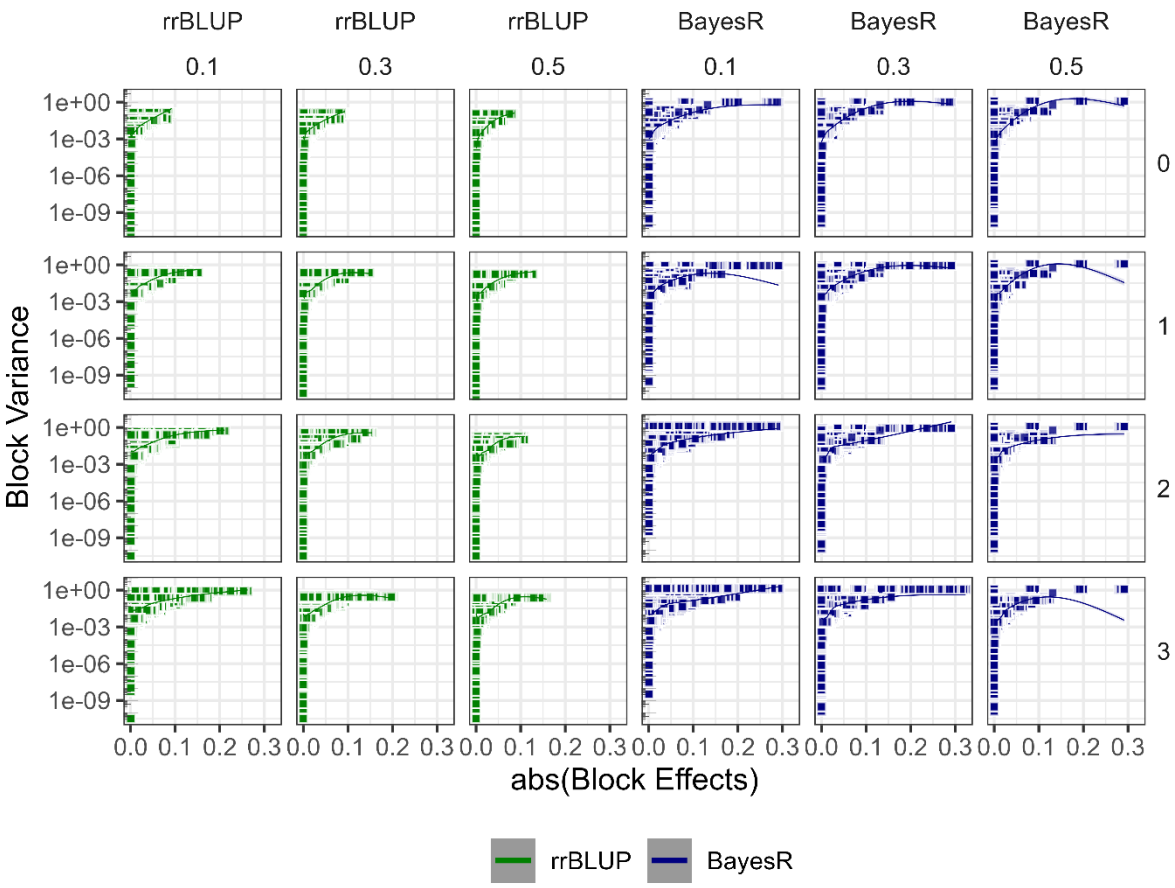

Supplementary Figure 3. Relationship between haploblock variance and haplotype effects using generalised additive model. Haploblock variance was determined from the localGEBV estimates using rrBLUP (*green*) and BayesR (*blue*); and plotted as min-max scaled of the $\log_{10}$ transformed variance for visual clarity. Haplotype effect is equivalent to localGEBV, which is the sum of SNP marker effects within haploblocks. In the figure, different LD parameters are shown as facets: *column facet* represented by LD threshold at $r^2 \in \{0.1,0.3,0.5\}$; and *row facet* as marker $tol \in \{0,1,2,3\}$.

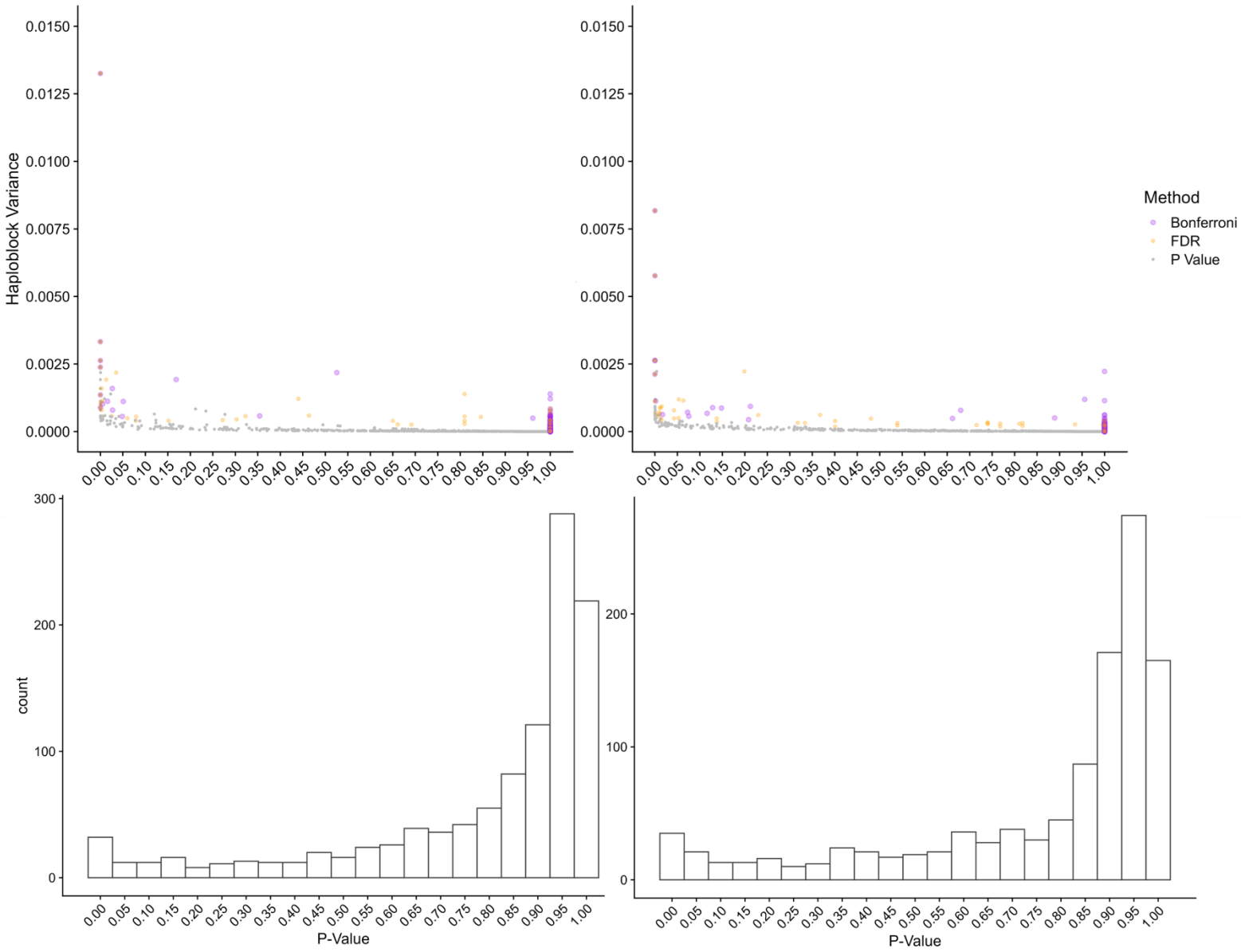
Haploblock Variance
0.0150
0.0125
0.0100
0.0075
0.0050
0.0025
0.0000
0.00 0.05 0.10 0.15 0.20 0.25 0.30 0.35 0.40 0.45 0.50 0.55 0.60 0.65 0.70 0.75 0.80 0.85 0.90 0.95 1.00
Method
Bonferroni
FDR
P Value
count
300
200
100
0
P-Value

1196

1197 **Supplementary Figure 4. Characterisation of the distribution of p-values and their relationship to haploblock variance**. (**A**) The
1198 relationship between haploblock variance calculated using BayesR, p-values, and p-values adjusted with Bonferroni or False Discovery Rate
1199 (FDR) multiple testing correction. (**B**) The relationship between haploblock variance calculated using rrBLUP, p-values, and p-values adjusted
1200 with Bonferroni or FDR multiple testing correction. (**C**) The distribution of unadjusted p-values calculating haploblock variance with BayesR
1201 marker effects. (**D**) The distribution of unadjusted p-values calculating haploblock variance with rrBLUP marker effects.

1202

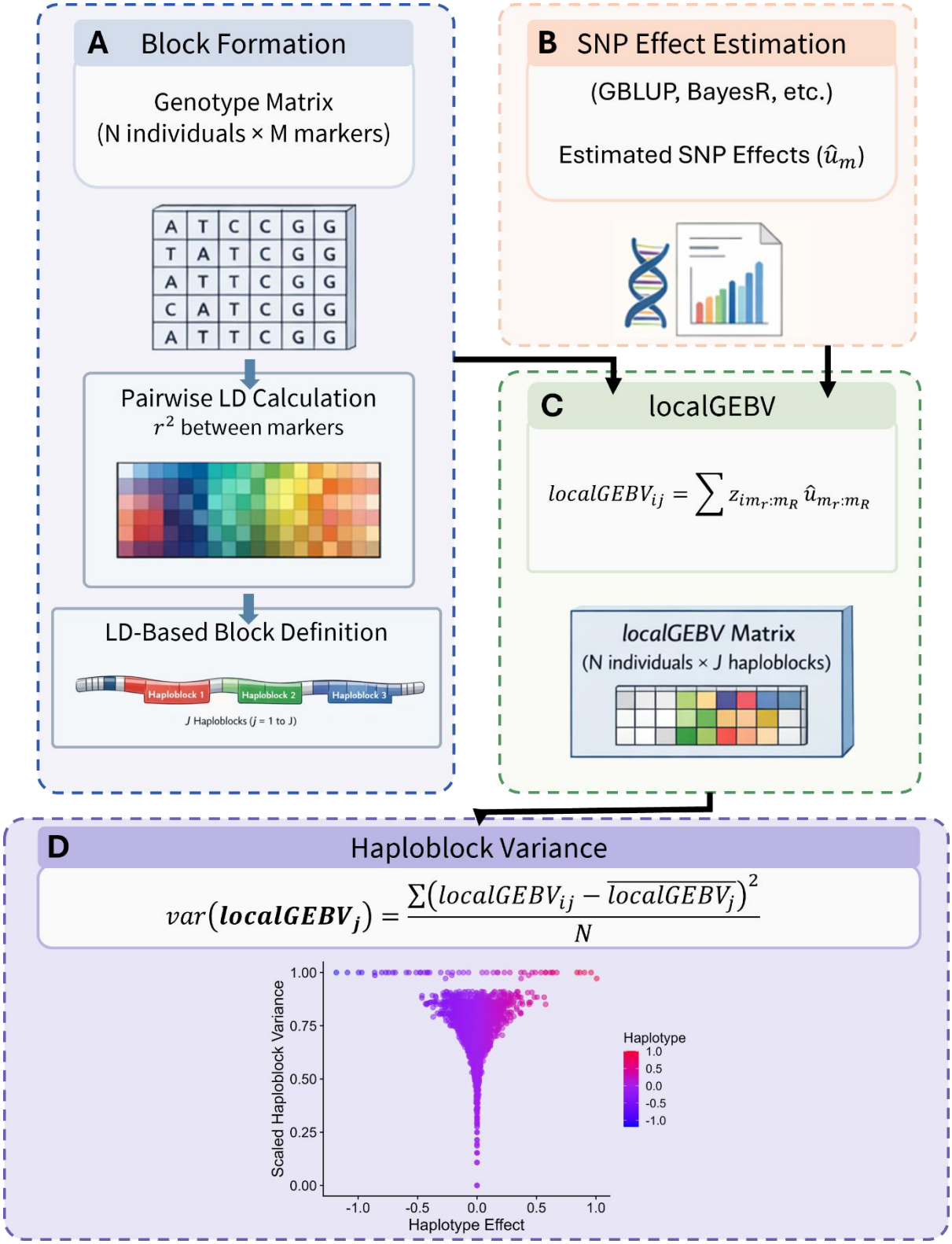

Supplementary Figure 5. Diagram of the localGEBV process. The localGEBV process consists of three computing steps and a summarization step: (**A**) block formation from pairwise LD between M markers, (**B**) SNP effect estimation, (**C**) calculating localGEBV of all N individuals (denoted by i) for all j individual haploblocks in J, and (**D**) computing the variance of all j individual haploblocks in J (tornado plot is for demonstration purposes only).